



# Impact of tropical cyclones over the eastern North Pacific on El Niño–Southern Oscillation intensity

Qiuyun Wang<sup>1</sup> · Zhe-Min Tan<sup>1</sup>

Received: 24 June 2022 / Accepted: 16 February 2023 / Published online: 6 March 2023  
© The Author(s), under exclusive licence to Springer-Verlag GmbH Germany, part of Springer Nature 2023

## Abstract

Most tropical cyclones (TCs) generated over the eastern North Pacific (ENP) do not make landfall. Consequently, TCs in this basin have received less attention, especially those that occur away from the mainland. Furthermore, there have been few studies of the climatic effects of ENP TCs. This study explores the feedback relationship between ENP TCs and the intensity of the El Niño–Southern Oscillation (ENSO), including El Niño and La Niña events, from the perspective of accumulated cyclone energy (ACE). Observational and modeling results indicate that the ENP ACE 3 months earlier can still affect the intensity of El Niño and La Niña events, although the SST persistence is main contributor. Thereinto, the impact of ENP TCs on El Niño appears to be approximately equal to that on La Niña. Moreover, this impact is independent of the persistence of the sea surface temperature (SST) in the Niño 3.4 region and the Madden–Julian Oscillation. Generally, the greater the ENP ACE, the stronger the El Niño, and the smaller the ENP ACE, the stronger the La Niña; this is especially the case for those TCs that develop over the July–September period. In addition, results show that the ENP TCs modulate ENSO intensity by changing anomalous zonal wind at the low-level atmospheric layer. And the joint impacts of the low-level zonal wind anomalies on the Walker circulation and the east–west thermocline gradient lead to the time characteristics that ENP TCs lead ENSO intensity by about 3 months.

**Keywords** Tropical cyclones · Accumulated cyclone energy · ENSO · Intensity · Eastern North Pacific

## 1 Introduction

El Niño and La Niña events, the warm and cool phases of the El Niño–Southern Oscillation (ENSO, all abbreviations occurred in the text or figures have been shown in the Appendix I), have a tremendous impact on global synoptic and climatic systems (Alexander et al. 2002; Kug et al. 2009; Feng and Li 2011; Wang et al. 2016, 2019b; Xie et al. 2020). As the second most active ocean basin with respect to tropical cyclones (TCs), the eastern North Pacific (ENP) experiences ~ 17% of all TCs worldwide (Li et al. 2016). As in the other basins (Camargo and Sobel 2005; Chand et al. 2013; Wang et al. 2013; Zhan et al. 2017; Guo and Tan 2018; Yang and Oh 2018; Kim et al. 2020), ENSO has a significant influence on TC activity over the ENP, and especially on those

TCs that develop in the western portions of the ENP (Chu and Wang 1997; Irwin and Davis 1999; Chu 2004; Camargo et al. 2008; Gutzler et al. 2013; Jin et al. 2014; Jien et al. 2015; Balaguru et al. 2020). Compared with La Niña events, during El Niño events, the number of westward-moving TCs increases, and the average genesis location of the ENP TCs is more westward. These TCs also have greater intensity and longer lifespans. Hence, during these periods, most TCs are away from the North American coastline, and the incidence of TCs in the vicinity of Hawaii increases.

In addition to the modulation of TC activity by ENSO, observational and modeling studies have shown that TCs can also affect the sea surface temperature (SST) in the ENP (Keen 1982; Fedorov et al. 2010; Lian et al. 2019; Wang et al. 2019b). Some studies of TC cases have suggested that this influence might result from the modulation by TCs of westerly wind bursts and the propagation of equatorial oceanic waves (Sriver et al. 2013; Lian et al. 2018). On interannual timescales, Camargo and Sobel (2005) found firstly that accumulated cyclone energy (ACE; Bell et al. 2000) over the western North Pacific leads Niño indices. Furthermore,

✉ Zhe-Min Tan  
zmtan@nju.edu.cn

<sup>1</sup> Key Laboratory of Mesoscale Severe Weather/Ministry of Education and School of Atmospheric Sciences, Nanjing University, Nanjing 210023, China

Wang et al. (2019b) showed that ACE is a key bridge between TCs and climatic events, and they demonstrated systematically that TCs over the western North Pacific can affect El Niño intensity by modulating the Walker circulation and equatorial oceanic kelvin waves. In addition, recent study has demonstrated that TCs over the western North Pacific can affect the spatial pattern of ENSO (Wang and Li 2022a, b, c).

To sum up, previous studies have demonstrated that TCs play an important role in climatic events, but studies of the climatic effect of TCs on ENSO have focused mainly on TCs over the western North Pacific. Furthermore, because most TCs over the ENP do not make landfall, the TCs that develop in this basin have received less attention. Consequently, the primary purpose of this study is to investigate whether a feedback relationship exists between ENP TCs and ENSO intensity. In the remainder of the paper, Sect. 2 describes the data and methods used in our analysis, Sect. 3 provides evidence to verify the influence of the preceding (3 months earlier) TCs over the ENP on El Niño and La Niña intensity, and discusses the role of SST persistence in this influence, and Sect. 4 explores the role of the Madden–Julian Oscillation (MJO) with respect to the modulation of ENSO intensity by ENP TCs, Sect. 5 shows the possible mechanisms how the ENP TCs affect ENSO intensity. Finally, in Sect. 6, we present a summary of our key findings and our conclusions.

## 2 Data and methods

### 2.1 Data

The 6-h maximum sustained surface wind speeds and the locations of all recorded ENP TCs over the period 1970–2020 were obtained from the International Best Track Archive for Climate Stewardship (IBTrACS) maintained by the National Oceanic and Atmospheric Administration (NOAA); The daily SST data for the period 1979–2020 were obtained from the ERA5 dataset of European Centre for Medium-Range Weather Forecasts (ECMWF). We also used NOAA's interpolated outgoing longwave radiation (OLR) data for the period 1979–2020 (Liebmann and Smith 1996). The monthly wind dataset for the period 1970–2020, with a horizontal resolution of  $2.5^\circ \times 2.5^\circ$ , was obtained from the National Centers for Environmental Prediction–National Center for Atmospheric Research (NCEP–NCAR) reanalysis dataset (Kalnay et al. 1996). The monthly SST data were obtained from the Extended Reconstructed Sea Surface Temperature (ERSST) V5 dataset, with a horizontal resolution of  $2^\circ \times 2^\circ$  (Huang et al. 2017). Ocean variables are taken from the Simple Ocean Data Assimilation product (Carton and Giese 2008) for the period 1970–2010, with a horizontal

resolution of  $0.5^\circ \times 0.5^\circ$ . All monthly data were smoothed using a 3-month running mean.

### 2.2 Selection of ENSO events

According to the de-facto standard developed by NOAA, the Niño 3.4 index is defined as the running 3-month mean of the SST anomaly for the Niño 3.4 region ( $5^\circ\text{S}–5^\circ\text{N}$ ,  $120–170^\circ\text{W}$ ). 5 consecutive overlapping 3-month periods at or above the  $+0.5^\circ$  anomaly (at or below the  $-0.5^\circ$  anomaly) defines the El Niño (La Niña) events; and the threshold of the moderate events changes to  $\pm 1.0^\circ$  to  $\pm 1.4^\circ$  anomaly (<https://ggweather.com/enso/oni.htm>). For this study, we used above-moderate (including moderate) ENSO events. Consequently, the selected El Niño events were from the years 1972–1973, 1982–1983, 1986–1987, 1991–1992, 1994–1995, 1997–1998, 2002–2003, 2009–2010, and 2015–2016, and the selected La Niña events were from 1970–1971, 1973–1974, 1975–1976, 1988–1989, 1995–1996, 1998–1999, 1999–2000, 2007–2008, 2010–2011, 2011–2012, and 2020–2021. The maximums of the Niño 3.4 index for all of the events selected in this study occurred from October to January, therefore the El Niño event of 1987–1988 was excluded. The year in which the El Niño (La Niña) event developed from weak to strong (January–December) was used to classify the El Niño (La Niña) developing year, and the year in which the El Niño (La Niña) event decayed from strong to weak to classify the El Niño (La Niña) decaying year.

### 2.3 ACE

The ACE (Bell et al. 2000; Wang et al. 2019b; Wang and Li 2022a) in a single  $2^\circ$  latitude  $\times$   $2^\circ$  longitude grid cell ( $x, y$ ) was calculated as follows:

$$ACE(x, y) = \sum_i V_{\max}(x, y)_i^2, \quad (1)$$

where  $x$  and  $y$  are latitude and longitude, respectively,  $i$  is the  $i$ th TC in the grid cell ( $x, y$ ), and  $V_{\max}$  is the recorded maximum sustained surface wind speed (in knots) every 6 h. Thus, the ACE index in the key domain of the ENP ( $5^\circ–25^\circ\text{N}$ ,  $125^\circ\text{W}–180^\circ$ ) is defined as the anomaly of the sum of the ACE for all grid cells in this region. Figure 1 shows how the key domain of the ENP ACE was identified.

### 2.4 MJO index and events

The MJO is one of the dominant modes of variability in the tropical atmosphere over intraseasonal timescales (Madden and Julian 1972, 1994; Madden 1986). The two leading principal components (PCs) of the empirical orthogonal

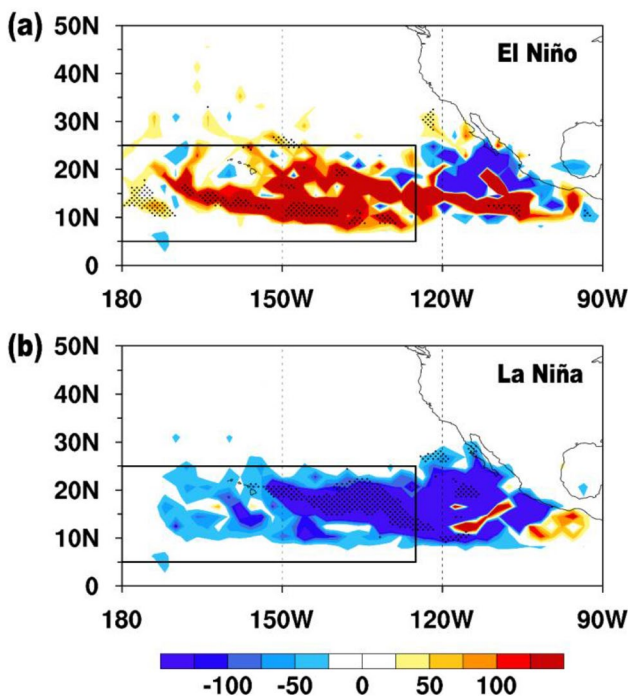


**Fig. 1** Composite of the ENP ACE anomalies (shading, knot<sup>2</sup>) during the developing years of **a** El Niño and **b** La Niña from 1970 to 2020. The black rectangle denotes the key domain of ACE (5°–25°N, 125°W–180°). The stippled regions indicate significance above the 95% confidence level, based on Student’s *t*-test

functions of OLR with a 30–60 days band-pass filtering are PC1 and PC2 (Wheeler and Hendon 2004), and the daily MJO index is calculated from  $PC1^2 + PC2^2$ . MJO events are defined as occurring when  $\sqrt{PC1^2 + PC2^2} \geq 1$ , and non-MJO events as occurring when  $\sqrt{PC1^2 + PC2^2} < 1$ . MJO events can be divided into two types based on their eight phases; i.e., active and inactive MJO events. Generally, phases 4–7 represent the active MJO events, and phases 1–3 and 8 represent the inactive MJO events.

**2.5 Explained percentage**

To quantify the contributions from the different impact factors, Wang et al. (2019b) defined the concept of explained percentage, which is calculated using regression analysis as follows.

Step 1. Obtain that part of *Y* associated with *X* ( $\tilde{Y}_X$ ):

$$\tilde{Y}_X = a_0X + a_1, \tag{2}$$

where  $a_0$  and  $a_1$  are the regression coefficient and a constant, respectively.

Step 2. The explained percentage ( $EP_X$ ) of  $\tilde{Y}_X$  for *Y* is:

$$EP_X = \frac{\tilde{Y}_X}{Y} \times 100\% \tag{3}$$

In addition, we can obtain the *X*-independent  $Y$  ( $Y_X^*$ ; that is, the remainder of *Y* after removing the signal of *X* or the signal of *X* is removed from the *Y*) after obtaining  $\tilde{Y}_X$ :

$$Y_X^* = Y - \tilde{Y}_X \tag{4}$$

In this study, all of regression analyses (i.e., Eq. 2) are based on the monthly datasets in the period 1970–2020 (1970–2010 for thermocline dataset) except for MJO. For MJO, the first step to obtain MJO-independent Niño 3.4 index is to remove the MJO signal from the daily SST data during 1979–2020. Then the processed daily SST data is transformed into monthly data. Thus, MJO-independent Niño 3.4 index can be obtained. It should also be noted that this study involves removing the autocorrelation of the Niño 3.4 index, which means removing the influence of the Niño 3.4 index on itself three months earlier. Therefore, the impact factor (*X*) is the Niño 3.4 index three months earlier.

After passing the significance test of regression analysis, the results during ENSO developing year are selected to composite. Then, take a statistical significance test for composite analysis, that is, to examine whether there is a significant difference between the ENSO developing year and all years, if it’s true, it means that the composite result is significant. Thus, we can obtain the corresponding explained percentages.

**2.6 Effective number of degrees of freedom**

The effective number of degrees of freedom ( $N^{eff}$ ) is used to calculate the statistical significance of the correlation between two autocorrelated time series and was assessed using a two-tailed Student’s *t* test (Pyper and Peterman 1998; Xie et al. 2014; Sun et al. 2015; Wang et al. 2019a):

$$\frac{1}{N^{eff}} \approx \frac{1}{N} + \frac{2}{N} \sum_{j=1}^N \frac{N-j}{N} \rho_{S1}(j)\rho_{S2}(j), \tag{5}$$

where *N* is the sample size and  $\rho_{S1}(j)$  and  $\rho_{S2}(j)$  are the autocorrelations of the two sampled time series *S1* and *S2*, respectively, at time lag *j*. In this study, the effective number of degrees of freedom is applied to calculate the statistical significance of the lead-lag correlations between *S1* and *S2*, including ACE and Niño 3.4 index, ACE and Walker circulation index, and ACE and the east–west thermocline gradient index, via the Student *t* test. Thereinto, Walker circulation index =  $U_{200} - U_{850}$ , where  $U_{200}$  and  $U_{850}$  are the mean zonal wind anomalies (5°S–5°N, 120°W–120°E) at the 200- and 850- hPa levels, respectively.

And the east–west thermocline gradient index =  $20\text{ }^{\circ}\text{C}$  isotherm depth $_{[5^{\circ}\text{S}-5^{\circ}\text{N}, 120^{\circ}\text{W}-170^{\circ}\text{W}]} - 20\text{ }^{\circ}\text{C}$  isotherm depth $_{[5^{\circ}\text{S}-5^{\circ}\text{N}, 120^{\circ}\text{E}-170^{\circ}\text{E}]}$ . Unless otherwise stated, all datasets are the monthly data in the period 1970–2020 (1970–2010 for thermocline dataset).

## 2.7 Model and design of experiments

In the part which the relative contributions of the different impact factors are discussed, an intermediate-complexity coupled ocean–atmosphere model (Zebiak and Cane 1987; Chen et al. 2000, 2004; Gao et al. 2020), LDEO<sub>5</sub>, is employed to verify the role of ENP ACE in affecting ENSO intensity. LDEO<sub>5</sub> model includes two modules: atmospheric and oceanic modules. And atmospheric dynamics are driven by steady state and linear shallow-water equations (Gill 1980), which can simulate the response of anomalous wind field to surface heat flux. The atmospheric module is on the grid resolution of  $2^{\circ}$ (latitude)  $\times$   $5.625^{\circ}$ (longitude), with the domain of  $29^{\circ}\text{S} - 29^{\circ}\text{N}$ ,  $101.25^{\circ} - 286.875^{\circ}\text{E}$ ; The oceanic dynamics are governed by a reduced-gravity model, which can simulate the response of upper ocean to anomalous wind field. The oceanic module is on the grid resolution of  $2^{\circ}$ (latitude)  $\times$   $0.5^{\circ}$ (longitude), with the domain of  $28.75^{\circ}\text{S} - 28.75^{\circ}\text{N}$ ,  $124^{\circ} - 280^{\circ}\text{E}$ . More details of LDEO<sub>5</sub> have been reported in the previous study (Chen et al. 2004). This model has been widely applied to study the response of ENSO to the different external forces (Wang et al. 2019b; Gao et al. 2020). In this study, eight experiments are set up, details can be found in the Appendix II.

## 3 The feedback relationship between ENP ACE and ENSO events

### 3.1 Timeseries characteristics

As shown in Fig. 1, the change in the mean ACE anomalies is evident to the west of  $125^{\circ}\text{W}$  during the ENSO developing years. Furthermore, during the El Niño developing years (Fig. 1a), the ACE anomalies are greater than those seen in the climatology, which might be associated with the westward shift of the TC genesis location and tracks (Chu and Wang 1997; Chu 2004; Camargo et al. 2008). The opposite situation occurs during the La Niña developing years; i.e., the ACE anomalies are less than those seen in the climatology (Fig. 1b). Based on this distribution, the ACE in the key domain ( $5^{\circ} - 25^{\circ}\text{N}$ ,  $125^{\circ}\text{W} - 180^{\circ}$ ; hereafter ENP ACE) was selected for further study. The results of the lead–lag correlation analysis (Fig. 2a) indicate that ENP ACE leads the Niño 3.4 index by about 3 months reaching its maximum (correlation coefficient is  $\sim 0.32$ ). Meanwhile, the simultaneous correlation coefficient between ENP ACE and Niño 3.4

index reaches  $\sim 0.23$ , and this correlation coefficient is also significant although it's weak. These relationships imply that the strong autocorrelation of SST in the Niño 3.4 region (i.e., SST persistence) might be the main reason why ENP ACE leads the Niño 3.4 index. As shown in Fig. 2a, differing from the Niño 3.4 index, the autocorrelation of ENP ACE with its value 3 months earlier is not significant. The whole variation of the autocorrelation of ENP ACE also differs from that of the Niño 3.4 index (Fig. 2a). Moreover, when the preceding Niño 3.4 index is removed from ENP ACE, ENP ACE still leads the Niño 3.4 index (Fig. 2b). Even after removing the autocorrelation of the Niño 3.4 index with its value 3 months earlier, this lead relationship is still evident (Fig. 2b). Of course, there is another problem, when the ENP ACE leads the Niño 3.4 index by about 3 months, the correlation coefficient between them is  $\sim 0.32$ . It seems a little weak. Actually, it results from the few TCs in non-ENSO year. The result from the lead-lag correlation between the ENP ACE and Niño 3.4 index during the ENSO developing year further verifies this point, the correlation coefficient can reach up to  $\sim 0.48$  when ACE leads Niño 3.4 index by 3 months (Fig. 2c); when the preceding Niño 3.4 index is removed from ENP ACE, ENP ACE still leads the Niño 3.4 index (Fig. 2d), and the correlation coefficient changes a little before and after the removal of the preceding Niño 3.4 index. Even after removing the autocorrelation of the Niño 3.4 index with its value 3 months earlier, this lead relationship is still evident (Fig. 2d). All of these features imply that the influence of the preceding ENP ACE on the Niño 3.4 index does not result entirely from the persistence of SST in the Niño 3.4 region.

However, aforementioned correlativity analysis is not enough to demonstrate the extent of effects of the preceding Niño 3.4 index on the feedback relationship between the preceding ENP ACE and SST in the Niño 3.4 region. As shown in Fig. 3a, when the preceding Niño 3.4 index is removed, the intensity of the preceding ENP ACE changes very little, but the intensity of Niño 3.4 index related to the preceding ACE is weakened (Fig. 3b). This result verifies that the change in the preceding Niño 3.4 index is important to the intensity of the Niño 3.4 index. When ENP ACE is removed, the intensity of the Niño 3.4 index seems to change little (Fig. 3c), as does the related Niño 3.4 index 3 months later (Fig. 3d). That is, the persistence of SST in the Niño 3.4 region seems to be relatively unaffected by ENP ACE. Actually, after removing the preceding ENP ACE, the change in persistence of SST in the Niño 3.4 region is significant during El Niño and La Niña developing years (Figs. 3c–d), and Tables 1 and 2 show the more details. During El Niño (Table 1) and La Niña (Table 2) developing years, the persistence of SST in the Niño 3.4 region after removing the preceding ENP ACE changes noticeably. During ENSO developing years, the greater the absolute value of the ENP ACE

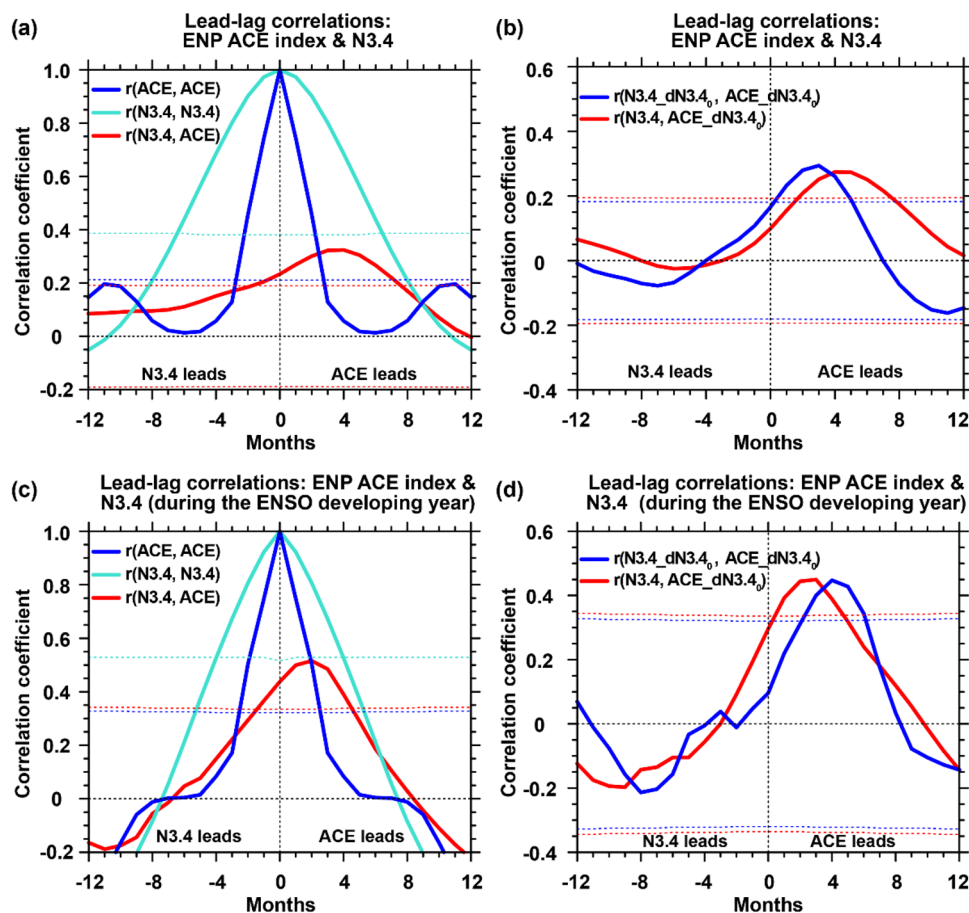


**Fig. 2** Lead–lag correlations between the ENP ACE anomalies ( $5^{\circ}$ – $25^{\circ}$ N,  $125^{\circ}$ W– $180^{\circ}$ ) and the Niño 3.4 index together with their auto-correlations for the period 1970–2020. In **a**, red, turquoise and blue solid lines indicate the correlations between the Niño 3.4 index and ENP ACE, and the autocorrelations of the Niño 3.4 index and ENP ACE, respectively. Red, turquoise and blue dashed lines indicate the corresponding significance at the 99% confidence level based on Student's  $t$ -test using the effective number of degrees of freedom. In **b**, some series of the Niño 3.4 index and ACE are processed. The details

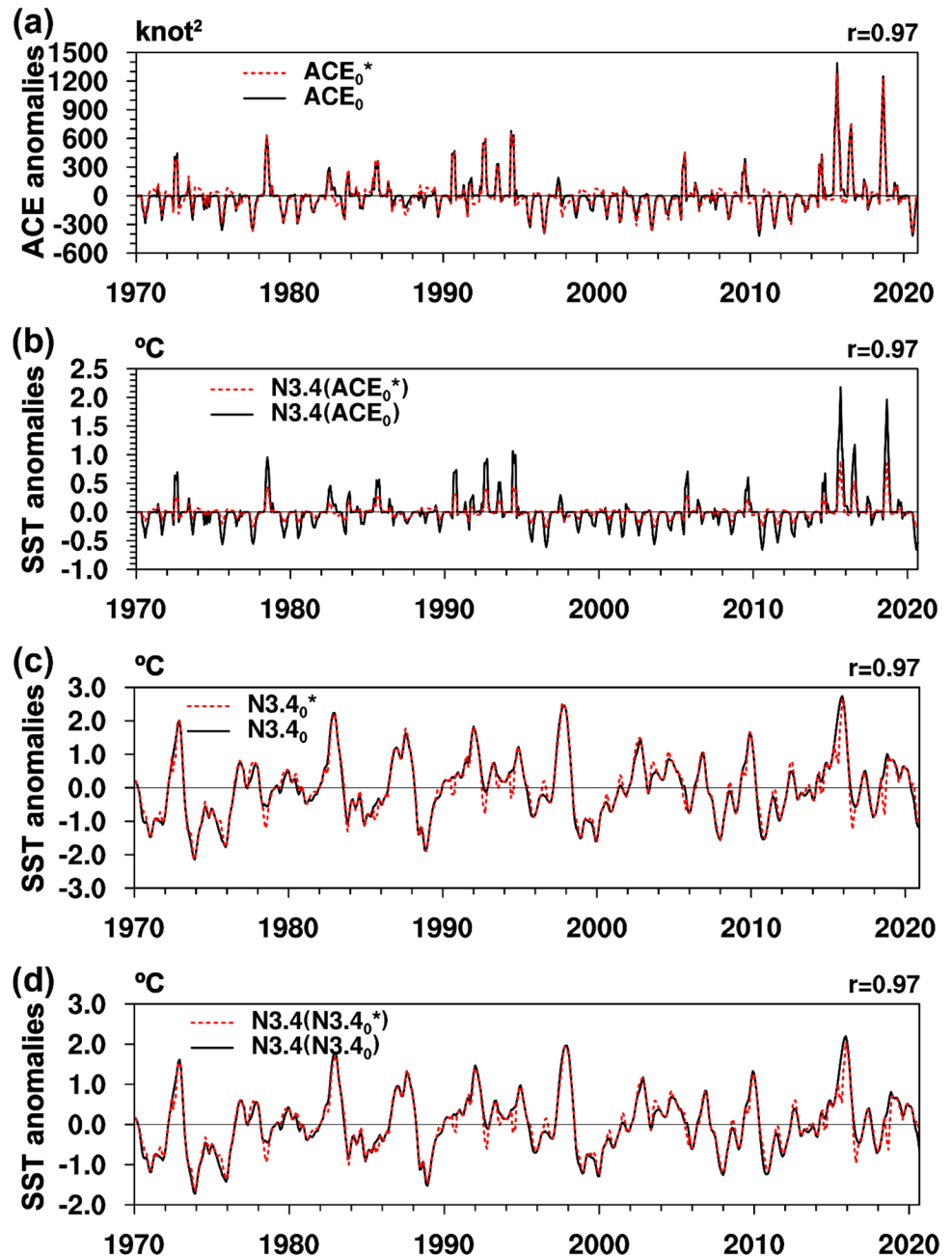
are as follows, N3.4 indicates the original series; N3.4\_dN3.4<sub>0</sub> and ACE\_dN3.4<sub>0</sub> denote the Niño 3.4 index and ENP ACE, respectively, which the preceding (3 months earlier) Niño 3.4 index is removed. Red, blue solid lines indicate the lead–lag correlations between N3.4 and ACE\_dN3.4<sub>0</sub>, N3.4\_dN3.4<sub>0</sub> and ACE\_dN3.4<sub>0</sub>, respectively. Dashed lines are the corresponding significance at the 99% confidence level. **c**, **d** are same as **a** and **b**, but for the Niño 3.4 index and ACE anomalies during the ENSO developing year

anomalies, the larger the change in the persistence of SST in the Niño 3.4 region before and after the removal of ENP ACE. This feature means the correlation between the Niño 3.4 index and its value 3 months earlier is closely linked to ENP ACE 3 months earlier during ENSO developing years. Generally, the greater the preceding ENP ACE, the stronger the El Niño, and the smaller the preceding ENP ACE, the stronger the La Niña.

To further explore this relationship among the Niño 3.4 index, the preceding ENP ACE, and the preceding Niño 3.4 index, the composites of the Niño 3.4 index during El Niño (Fig. 4a–f) and La Niña (Fig. 4g–l) events are shown in Fig. 4. We see that the contribution from the preceding Niño 3.4 index to the Niño 3.4 index decreases after removing the preceding ACE (Fig. 4a, b and g, h). Also, in accordance with the relationship between the Niño 3.4 index and the

preceding ACE, the contribution of the preceding ACE to the Niño 3.4 index decreases after removing the preceding Niño 3.4 index (Fig. 4c, d and i, j). The joint contribution of the preceding ACE and Niño 3.4 index to the Niño 3.4 index is greater than that of either factor alone (Fig. 4e and k), and the similar results are obtained when the joint contribution of the preceding Niño 3.4 index-independent ACE and Niño 3.4 index is checked (Fig. 4f and l). Moreover, both the joint contributions of the preceding ACE and ACE-independent Niño 3.4 index, and the preceding Niño 3.4 index-independent ACE and ACE-independent Niño 3.4 index are still similar to the joint contribution of the preceding ACE and Niño 3.4 index (Figures are not shown). These features mean that ENP ACE and SST persistence both play the roles in the development of the ENSO intensity in deed, and the contributions of ENP ACE and SST persistence are not simple

**Fig. 3** Time series of the **a** ENP ACE anomalies ( $\text{knot}^2$ ) and **b–d** Niño 3.4 index ( $^{\circ}\text{C}$ ). In **(a)**,  $\text{ACE}_0$  denotes the preceding ENP ACE anomalies.  $\text{ACE}_0^*$  indicates the preceding ENP ACE anomalies after removing the preceding Niño 3.4 index. In **(b)**,  $\text{N3.4}(\text{ACE}_0)$  and  $\text{N3.4}(\text{ACE}_0^*)$  indicate the Niño 3.4 indices associated with  $\text{ACE}_0$  and  $\text{ACE}_0^*$ , respectively. In **(c)**,  $\text{N3.4}_0$  denotes the preceding Niño 3.4 index, and  $\text{N3.4}_0^*$  indicates the preceding Niño 3.4 index after removing the preceding ENP ACE. In **(d)**,  $\text{N3.4}(\text{N3.4}_0)$  and  $\text{N3.4}(\text{N3.4}_0^*)$  indicate the Niño 3.4 indices associated with  $\text{N3.4}_0$  and  $\text{N3.4}_0^*$ , respectively.  $r$  is correlation coefficient. Statistical significance of regression and correlation analyses are both above the 95% confidence level



linear superposition. Previous studies have demonstrated that the intermediate-complexity coupled ocean–atmosphere model, LDEO<sub>5</sub>, can capture well the variations of the Niño 3.4 index (Zebiak and Cane 1987; Chen et al. 2004; Wang et al. 2019b). Consequently, we used this model to further examine the above results (Fig. 5). The model results were similar to the observations. It should be clarified that the error between the observations and modeling with respect to the Niño 3.4 index is greater during La Niña events than El Niño events, particularly during the decaying ENSO year, but the modeling results can still be useful for comparing the relative contributions of the different factors. These features

imply that the preceding ENP ACE can affect ENSO intensity, particularly for TCs over the July–September (J–A–S) period.

We also calculated the explained percentages of the different factors (including the Niño 3.4 index, ACE, ACE-independent Niño 3.4 index, Niño 3.4 index-independent ACE, the factor consists of ENP ACE and Niño 3.4 index, and the factor consists of Niño 3.4 index-independent ACE and Niño 3.4 index) for the J–A–S period. For El Niño events (Fig. 6a), the mean explained percentages of the Niño 3.4 index and ENP ACE during J–A–S relative to the Niño 3.4 index in October–December (O–N–D) are around 51%

**Table 1** ENP ACE anomalies from May to September (knot<sup>2</sup>, black) and the difference between N3.4(N3.4<sub>0</sub>) and N3.4(N3.4<sub>0</sub><sup>\*</sup>) (°C, black italic) from August to December during El Niño developing years. N3.4<sub>0</sub> denotes the preceding Niño 3.4 index. N3.4<sub>0</sub><sup>\*</sup> indicates the preceding Niño 3.4 index after removing the preceding ENP ACE. And N3.4(N3.4<sub>0</sub>) and N3.4(N3.4<sub>0</sub><sup>\*</sup>) indicate the Niño 3.4 indices are associated with N3.4<sub>0</sub> and N3.4<sub>0</sub><sup>\*</sup>, respectively

El Niño		5 (8)	6 (9)	7 (10)	8 (11)	9 (12)
1972	ACE	- 9.95	- 143.38	406.57	355.89	443.27
	<i>Diff</i>	<i>0.01</i>	<i>- 0.10</i>	<i>0.39</i>	<i>0.35</i>	<i>0.43</i>
1982	ACE	- 9.95	96.50	254.73	293.24	164.58
	<i>Diff</i>	<i>0.01</i>	<i>0.11</i>	<i>0.25</i>	<i>0.29</i>	<i>0.19</i>
1986	ACE	- 9.95	144.54	45.38	59.70	- 147.53
	<i>Diff</i>	<i>- 0.02</i>	<i>0.12</i>	<i>0.04</i>	<i>0.06</i>	<i>- 0.11</i>
1991	ACE	110.41	- 23.02	- 51.97	- 197.77	126.43
	<i>Diff</i>	<i>0.11</i>	<i>0.00</i>	<i>- 0.02</i>	<i>- 0.15</i>	<i>0.14</i>
1994	ACE	8.39	677.04	547.70	633.57	- 66.58
	<i>Diff</i>	<i>0.02</i>	<i>0.60</i>	<i>0.49</i>	<i>0.57</i>	<i>- 0.03</i>
1997	ACE	- 7.72	101.68	188.54	128.80	- 20.78
	<i>Diff</i>	<i>0.02</i>	<i>0.13</i>	<i>0.22</i>	<i>0.18</i>	<i>0.06</i>
2002	ACE	- 4.17	- 114.48	- 166.17	- 260.24	- 158.60
	<i>Diff</i>	<i>0.01</i>	<i>- 0.07</i>	<i>- 0.11</i>	<i>- 0.19</i>	<i>- 0.10</i>
2009	ACE	- 9.95	- 53.41	245.44	239.61	384.82
	<i>Diff</i>	<i>0.00</i>	<i>- 0.03</i>	<i>0.23</i>	<i>0.23</i>	<i>0.36</i>
2015	ACE	14.49	30.28	683.45	880.77	1387.80
	<i>Diff</i>	<i>0.05</i>	<i>0.07</i>	<i>0.65</i>	<i>0.83</i>	<i>1.29</i>

Italic represents diff values

*Diff*=N3.4(N3.4<sub>0</sub>) - N3.4(N3.4<sub>0</sub><sup>\*</sup>), and the numbers 5–12 in the first row represent May–December, respectively

**Table 2** As in Table 1, but for La Niña developing years

La Niña		5 (8)	6 (9)	7 (10)	8 (11)	9 (12)
1970	ACE	0.56	- 132.87	- 180.69	- 285.63	- 177.65
	<i>Diff</i>	<i>- 0.01</i>	<i>- 0.13</i>	<i>- 0.19</i>	<i>- 0.28</i>	<i>- 0.19</i>
1973	ACE	26.12	151.53	5.11	- 125.39	- 250.39
	<i>Diff</i>	<i>0.00</i>	<i>0.09</i>	<i>- 0.04</i>	<i>- 0.16</i>	<i>- 0.28</i>
1975	ACE	- 9.95	- 132.28	- 277.69	- 358.49	- 280.96
	<i>Diff</i>	<i>- 0.04</i>	<i>- 0.16</i>	<i>- 0.29</i>	<i>- 0.36</i>	<i>- 0.30</i>
1988	ACE	- 9.95	- 48.65	39.31	- 19.62	- 33.66
	<i>Diff</i>	<i>- 0.04</i>	<i>- 0.09</i>	<i>- 0.01</i>	<i>- 0.06</i>	<i>- 0.07</i>
1995	ACE	- 9.95	- 12.19	- 189.11	- 279.59	- 330.09
	<i>Diff</i>	<i>0.00</i>	<i>- 0.01</i>	<i>- 0.17</i>	<i>- 0.26</i>	<i>- 0.31</i>
1998	ACE	- 0.81	2.69	- 68.82	- 172.39	- 228.63
	<i>Diff</i>	<i>0.02</i>	<i>0.00</i>	<i>- 0.09</i>	<i>- 0.19</i>	<i>- 0.24</i>
1999	ACE	- 9.95	- 46.12	- 41.26	- 135.69	- 152.26
	<i>Diff</i>	<i>- 0.04</i>	<i>- 0.07</i>	<i>- 0.07</i>	<i>- 0.15</i>	<i>- 0.17</i>
2007	ACE	- 4.26	- 75.67	38.03	- 47.00	- 28.34
	<i>Diff</i>	<i>- 0.01</i>	<i>- 0.08</i>	<i>0.02</i>	<i>- 0.06</i>	<i>- 0.06</i>
2010	ACE	- 4.08	- 137.52	- 317.48	- 417.77	- 337.09
	<i>Diff</i>	<i>0.00</i>	<i>- 0.14</i>	<i>- 0.31</i>	<i>- 0.41</i>	<i>- 0.34</i>
2011	ACE	- 9.95	- 143.38	- 245.27	- 339.71	- 255.90
	<i>Diff</i>	<i>- 0.02</i>	<i>- 0.13</i>	<i>- 0.22</i>	<i>- 0.31</i>	<i>- 0.25</i>
2020	ACE	- 9.95	- 143.38	- 323.34	- 417.77	- 337.09
	<i>Diff</i>	<i>- 0.01</i>	<i>- 0.13</i>	<i>- 0.29</i>	<i>- 0.38</i>	<i>- 0.01</i>

Italic represents diff values

*Diff*=N3.4(N3.4<sub>0</sub>)-N3.4(N3.4<sub>0</sub><sup>\*</sup>), and the numbers 5–12 in the first row represent May–December, respectively

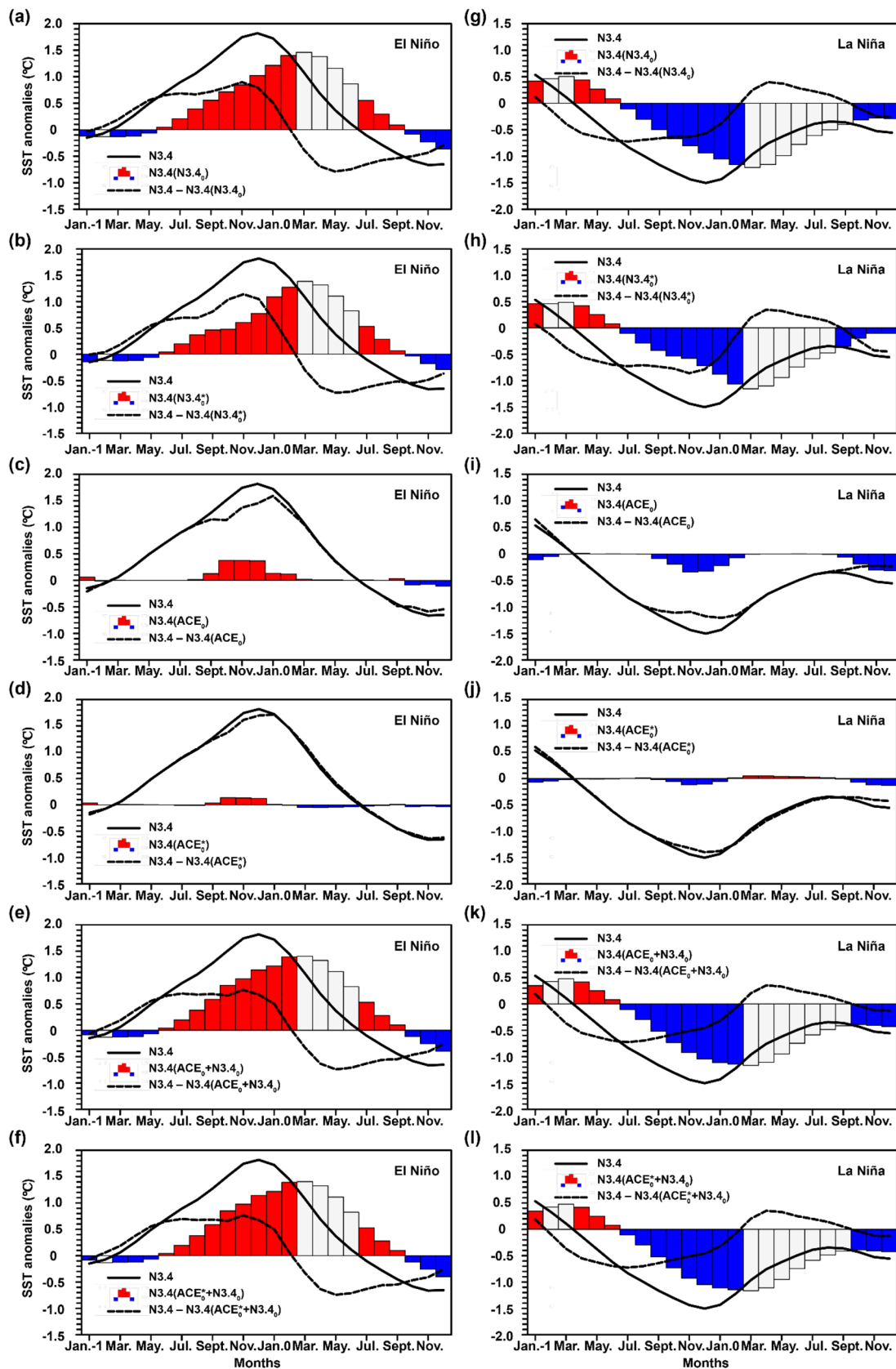




**Fig. 4** Time series of the Niño 3.4 index (lines, °C) for above-moderate El Niño and La Niña events (including moderate events), as well as the difference (bars, °C) between the original (solid lines) Niño 3.4 indices and preceding-contributor-independent events (dashed line) during the developing years (all months) of **a–f** El Niño and **g–l** La Niña.  $N3.4_0$  denotes the preceding Niño 3.4 index, and  $N3.4_0^*$  indicates the preceding Niño 3.4 index after removing the preceding ENP ACE.  $N3.4(N3.4_0)$  and  $N3.4(N3.4_0^*)$  indicate the Niño 3.4 indices associated with  $N3.4_0$  and  $N3.4_0^*$ , respectively.  $ACE_0$  denotes the preceding ENP ACE anomalies.  $ACE_0^*$  indicates the preceding ENP ACE anomalies after removing the preceding Niño 3.4 index.  $N3.4(ACE_0)$  and  $N3.4(ACE_0^*)$  indicate the Niño 3.4 indices associated with  $ACE_0$  and  $ACE_0^*$ , respectively.  $ACE_0 + N3.4_0$  represents the joint contribution of the preceding ENP ACE and Niño 3.4 index,  $N3.4(ACE_0 + N3.4_0)$  is the Niño 3.4 index associated with  $ACE_0 + N3.4_0$ .  $ACE_0^* + N3.4_0$  represents the joint contribution of the preceding  $ACE_0^*$  and Niño 3.4 index,  $N3.4(ACE_0^* + N3.4_0)$  is the Niño 3.4 index associated with  $ACE_0^* + N3.4_0$ . Red (blue) bars represent the positive (negative) differences between the original Niño 3.4 indices and preceding-contributor-independent events, whitesmoke bars indicate that the signals of the original Niño 3.4 indices are opposite to those from the preceding-contributor-independent events. Jan.–1 and Jan.0 represent the January in the developing and the decaying year of ENSO events, respectively. In **g–l**, the 2020–2021 La Niña event is not included because of the incomplete data from 2021. It must be pointed out that **a** is almost the same as Supplementary Fig. 4a in Wang et al. (2019b). Although the research period changed from 1970–2016 to 1970–2020, the number of El Niño events remained the same. Hence, it is necessary to mention this previous study here

(which is the same as the result in Wang et al. 2019b) and 22%, respectively. The mean explained percentages of the ACE-independent Niño 3.4 index and Niño 3.4 index-independent ACE during J–A–S relative to the Niño 3.4 index during O–N–D are approximately 36% and 8%, respectively. Both the joint explained percentages of the ENP ACE and Niño 3.4 index, and Niño 3.4 index-independent ACE and Niño 3.4 index during J–A–S are ~58%, which are greater than that of either factor alone (~7% more than the Niño 3.4 index and ~36% more than ENP ACE). The model generated similar results (Fig. 6b): the mean explained percentages of the Niño 3.4 index and ENP ACE during J–A–S relative to the Niño 3.4 index during O–N–D are approximately ~46% (also the same as Wang et al. 2019b) and ~16%, respectively. The mean explained percentages of the ACE-independent Niño 3.4 index and Niño 3.4 index-independent ACE during J–A–S relative to the Niño 3.4 index during O–N–D are approximately 34% and 6%, respectively. The joint explained percentages of the ENP ACE and Niño 3.4 index, and Niño 3.4 index-independent ACE and Niño 3.4 index during J–A–S are ~51%, which are also greater than that of either factor alone (~5% more than the Niño 3.4 index and ~35% more than ENP ACE). For La Niña events (Fig. 6c), the mean explained percentages of the Niño 3.4 index and ENP ACE during J–A–S relative to the Niño 3.4 index during O–N–D are approximately 59% and 19%, respectively. The mean explained percentages of the ACE-independent Niño

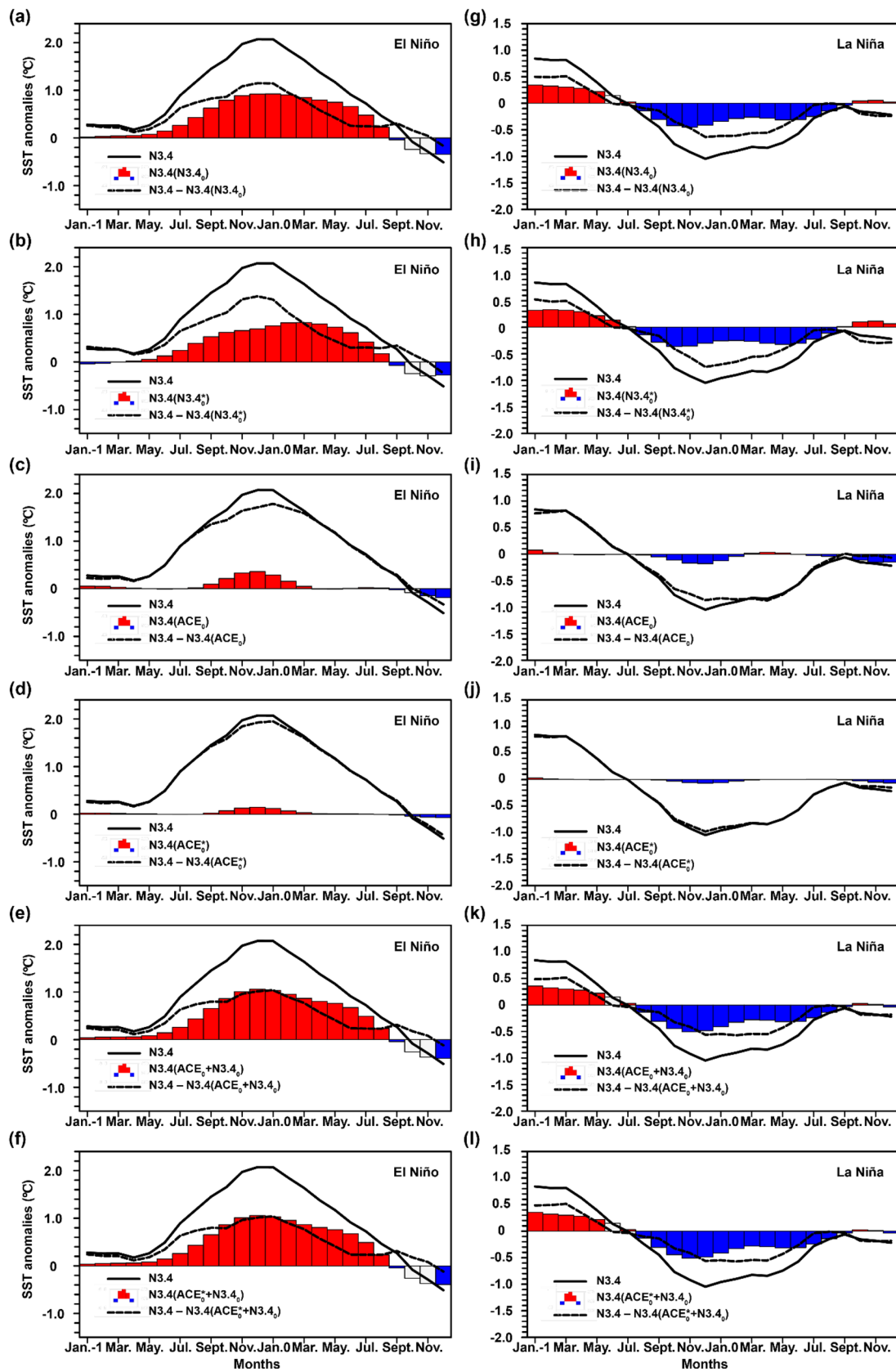
3.4 index and Niño 3.4 index-independent ACE during J–A–S relative to the Niño 3.4 index during O–N–D are about 46% and 6%, respectively. Both the joint explained percentages of the ENP ACE and Niño 3.4 index, and Niño 3.4 index-independent ACE and Niño 3.4 index during J–A–S are ~66%, which are greater than that of either factor alone (~7% more than the Niño 3.4 index and ~47% more than ENP ACE). As for the El Niño events, the model also generated similar results for the La Niña events (Fig. 6d): the mean explained percentages of the Niño 3.4 index and ENP ACE during J–A–S relative to the Niño 3.4 index during O–N–D are approximately 43% and 16%, respectively. The mean explained percentage of the ACE-independent Niño 3.4 index and Niño 3.4 index-independent ACE during J–A–S relative to the Niño 3.4 index during O–N–D are about 34% and 5%, respectively. The joint explained percentages of the ENP ACE and Niño 3.4 index, and Niño 3.4 index-independent ACE and Niño 3.4 index during J–A–S are both ~47%, which are greater than that of either factor alone (~4% more than the Niño 3.4 index and ~31% than ENP ACE).

Overall, our analysis of both the observations and model simulations demonstrates that the impact of the preceding ENP ACE on the Niño 3.4 index might be smaller than that of the preceding Niño 3.4 index (i.e., SST persistence), regardless of El Niño or La Niña events, but still cannot be ignored. Modulated extent of the J–A–S ENP TCs to the O–N–D Niño 3.4 index could reach ~7%–22% during El Niño, and ~6%–19% for La Niña. Here, it needs to be clarified that the minimum contributions are identified when the preceding Niño 3.4 index is supposed to be not affected by the preceding ACE at all. Actually, aforementioned analysis manifests the observed explained percentage of Niño 3.4 index decreases evidently after removing the influence of the preceding ACE (from 51 to 36% for El Niño, 59% to 46% for La Niña), i.e., the preceding ACE actually plays an important role in the preceding SST.

### 3.2 Spatial characteristics

More evidence of the modulation of ENSO intensity by the preceding ENP ACE can be found in the spatial distribution of SST anomalies related to ENP ACE. According to the results described above, ENP ACE during J–A–S has a significant influence on SST in the Niño 3.4 region 3 months later. Hence, we carried out further analysis regarding the spatial characteristics during these months.

For El Niño events (Fig. 7a–c), the O–N–D Niño 3.4 SST anomalies associated with the J–A–S ENP ACE capture well the spatial pattern of El Niño (Fig. 7a), and the intensity of the Niño 3.4 SST anomalies is strong. However, in contrast, the Niño 3.4 SST anomalies associated with the simultaneous ACE (Fig. 7b, c) are noticeably weaker. Furthermore,



◀**Fig. 5** As Fig. 4, but for the results from the model. Here, **a** is almost the same as Supplementary Fig. 4f in Wang et al. (2019b). Although the research period changed from 1970–2016 to 1970–2020, the number of El Niño events remained the same. Hence, it is necessary to mention this previous study here

if the impact of ENP ACE on the Niño 3.4 SST anomalies is caused by SST itself, according to the SST development associated with El Niño events, the O–N–D Niño 3.4 SST anomalies associated with the O–N–D ENP ACE should be stronger than the J–A–S Niño 3.4 SST anomalies associated with the J–A–S ENP ACE. However, the observations show the opposite, which is consistent with the strength of ENP ACE, and the mean of the ENP ACE anomalies during J–A–S ( $\sim 237.06 \text{ knot}^2$ ) is greater than that during O–N–D ( $\sim 57.52 \text{ knot}^2$ ). For La Niña events (Fig. 7d–f), the negative value of the Niño 3.4 SST anomalies associated with the simultaneous ACE (Fig. 7e, f) is evidently greater than the O–N–D Niño 3.4 SST anomalies associated with the J–A–S ENP ACE (Fig. 7d). That is, the intensity of the La Niña associated with the simultaneous ACE is weaker than that associated with the preceding ACE. Also, the intensity of the La Niña associated with the simultaneous ENP ACE during J–A–S is stronger than that during O–N–D, which is consistent with the comparison of the intensity of ENP ACE between J–A–S and O–N–D ( $\sim -199.16$  vs.  $\sim -65.52$

$\text{knot}^2$ ). Hence, these results further support the interpretation that the J–A–S ACE can significantly affect the O–N–D Niño 3.4 SST anomalies during El Niño and La Niña events. Therefore, the role of ENP ACE in the development of El Niño and La Niña events cannot be ignored.

### 4 Impact of the MJO on the modulation of ENSO intensity by ENP TCs

The MJO is known to be another main factor with respect to the development of ENSO and ENP TCs (Maloney and Hartmann 2000; Jiang et al. 2012; Boucharel et al. 2016; Puy et al. 2016). This study further explores the role of the MJO in the modulation of ENSO intensity by ENP TCs. Figure 8 shows the lead–lag correlation between the monthly Niño 3.4 index and ENP ACE. Firstly, when the SST data from the ERA5 dataset is used (in Fig. 2, the monthly SST is from NOAA’s ERSST V5), the strong correlation between ENP ACE and the Niño 3.4 index 3 months later is robust (Fig. 8a). Secondly, as can be seen from Fig. 8b, the relationship between ENP ACE and the Niño 3.4 index is hardly affected when the MJO signal is removed, and the amplitude of the correlation coefficient changes only slightly. That is, the MJO signal might not affect the modulation of ENSO intensity by ENP TCs over interannual timescales.

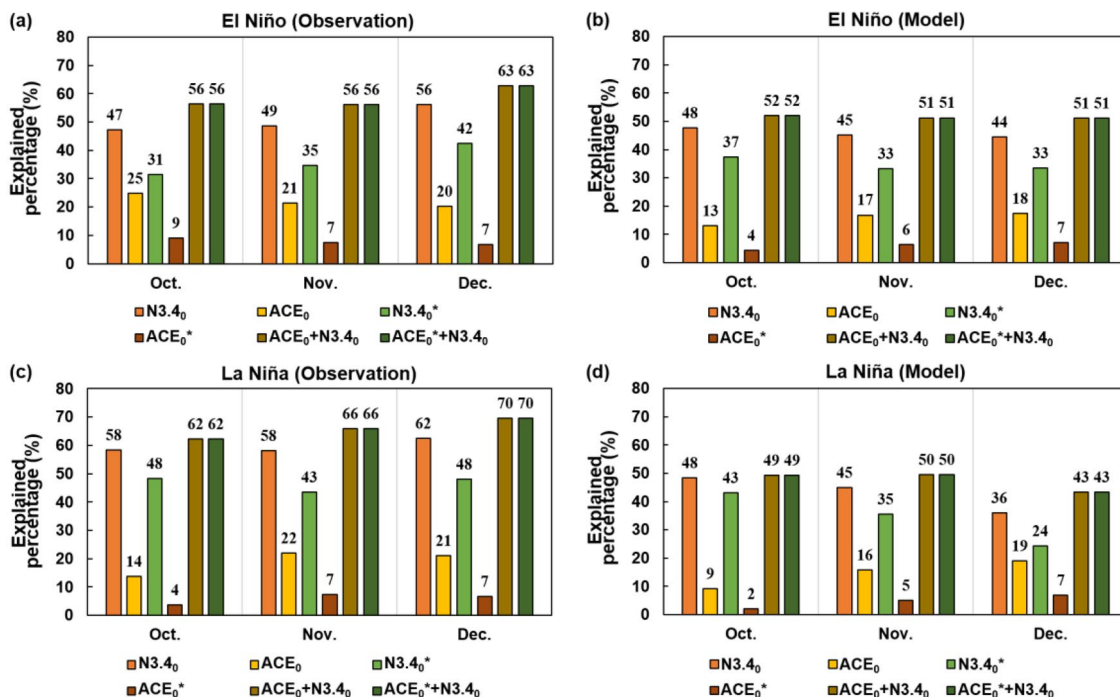


**Fig. 6** Explained percentage (%) of the Niño 3.4 index from October–December obtained using the J–A–S different contributors during (a, b) El Niño and (c, d) La Niña developing years (1970–2020). N3.4<sub>0</sub>, N3.4<sub>0</sub>\*, ACE<sub>0</sub>, ACE<sub>0</sub>\*, ACE<sub>0</sub>+N3.4<sub>0</sub> and ACE<sub>0</sub>\*+N3.4<sub>0</sub> are the Niño 3.4 index, the ACE-independent Niño 3.4 index, the ENP ACE, the

Niño 3.4 index-independent ACE, the factor consists of ENP ACE and Niño 3.4 index, and the factor consists of ENP ACE<sub>0</sub>\* and Niño 3.4 index in J–A–S, respectively. **a** and **c** are observations, **b** and **d** are the modeling results. Statistical significance of regression and composite analyses are both above the 95% confidence level

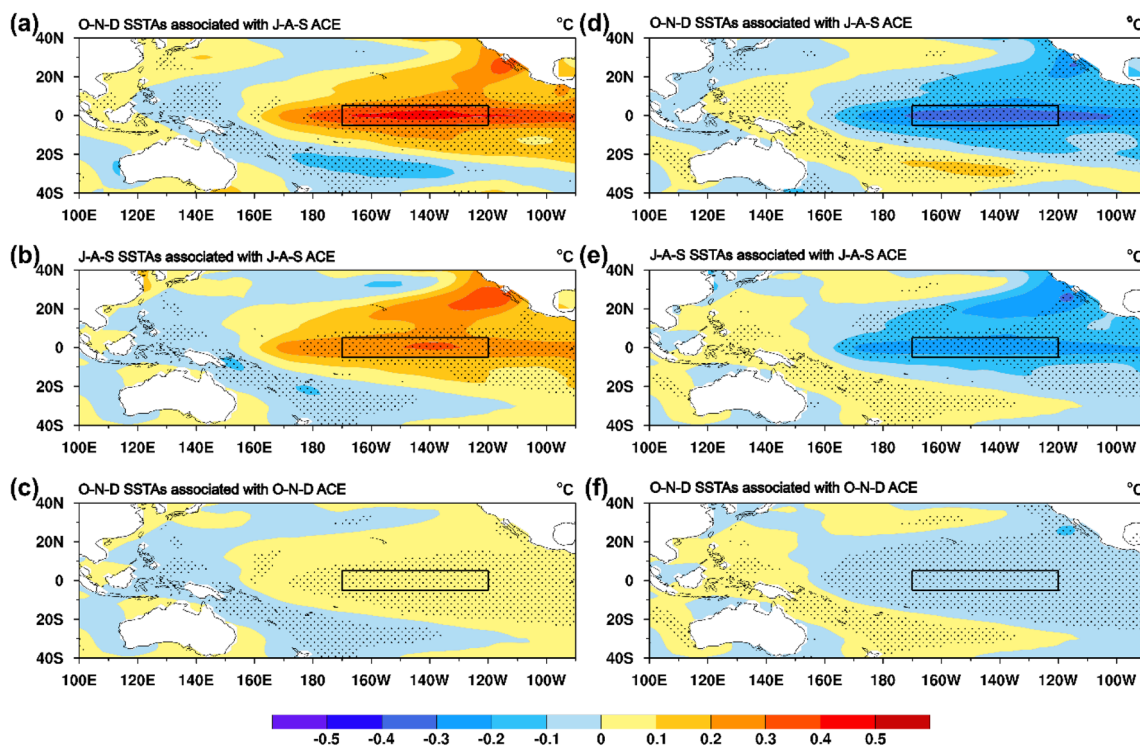


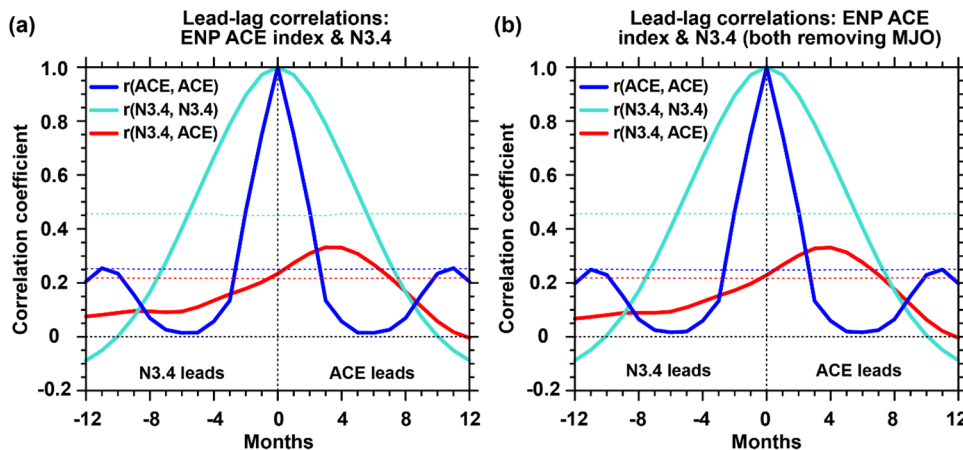
**Fig. 7** Composite of SST anomalies (shading, °C) associated with the ENP ACE during the developing year of El Niño and La Niña events over the period 1970–2020. **a** The O–N–D SST anomalies associated with the J–A–S ENP ACE during the El Niño developing years. **b** The J–A–S SST anomalies associated with the J–A–S ENP ACE during the El Niño developing years. **c** The O–N–D SST anomalies

associated with O–N–D ENP ACE during the El Niño developing years. The black rectangle denotes the Niño 3.4 region (5°S–5°N, 120°–170°W). Stippled regions denote the statistical significance of regression and composite analyses are both above the 95% confidence levels. **d–f** are same as **a–c**, but for La Niña events

It is not sufficient to check only the role of the MJO in the lead–lag relationship between ENP ACE and the Niño 3.4 index. The phases and events of the MJO might have more important impacts. The results in the Sect. 3 indicate that the J–A–S ENP TCs can significantly affect ENSO intensity during O–N–D. Hence, we first explored the relationship between the daily ENP TC activity and the MJO phases during J–A–S. For El Niño events, a previous study (Wang et al. 2019b) found that the occurrence frequency of

the eight MJO phases during J–A–S shows no significant difference, and this is also true for the occurrence frequency of the active MJO, inactive MJO, and non-MJO events. We used the same analysis for the La Niña events (Fig. 9), and the results also indicate that there are no evident differences in the occurrence frequency of the eight MJO phases during J–A–S. In addition, the differences among the occurrence proportions of the active and inactive MJO are not significant (Fig. 10): the mean occurrence proportion of active

**Fig. 8** **a** As Fig. 2a, but for the ERA5 dataset. **b** As **a**, but for the Niño 3.4 index and ENP ACE after removing the MJO index



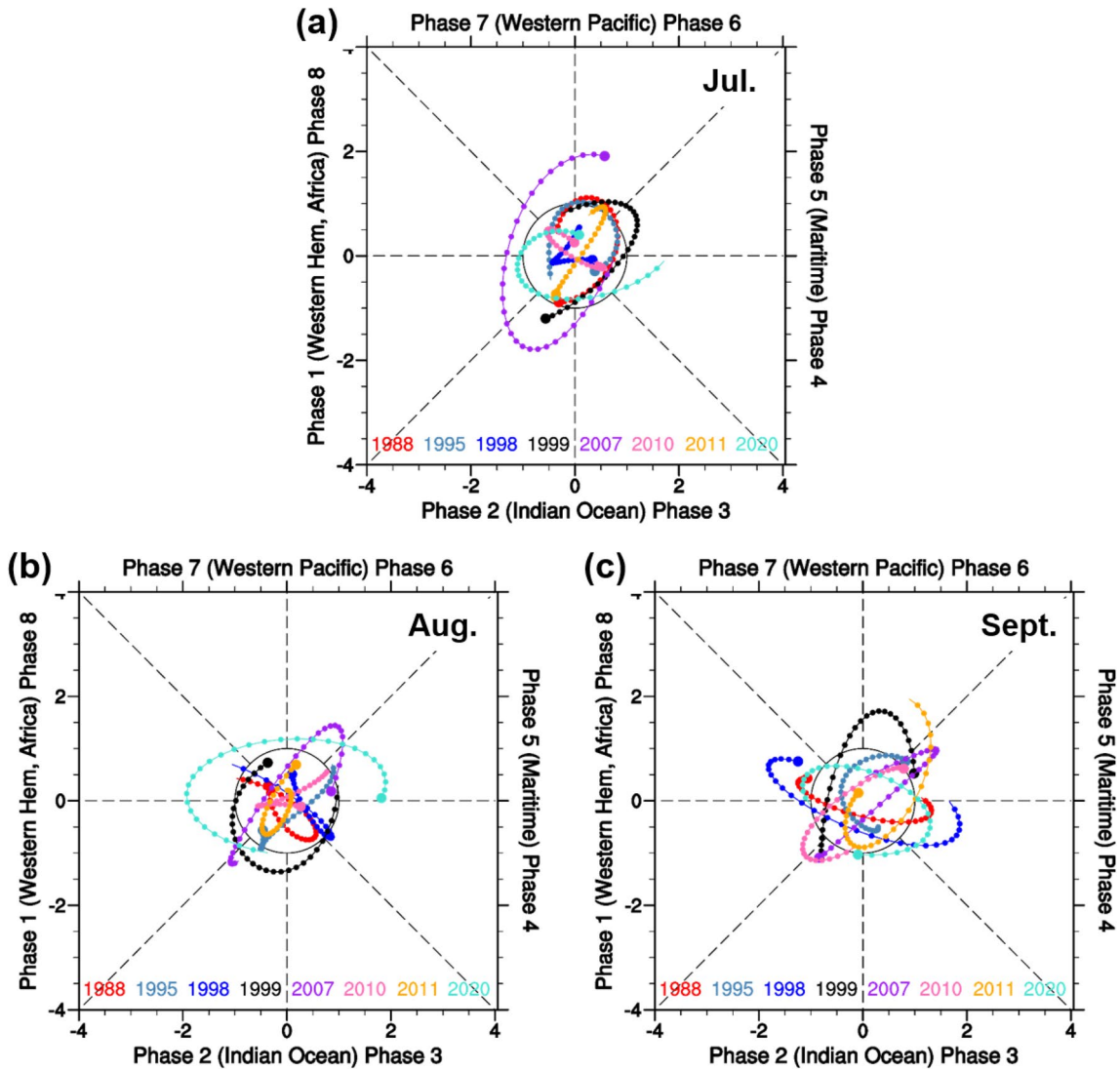


**Fig. 9** Phase distribution of the daily MJO indices in **a** July, **b** August, and **c** September during La Niña developing years over the period 1979–2020. Large dots indicate the first day of each month,

small dots are the remaining days in each month, and lines denote each La Niña developing year

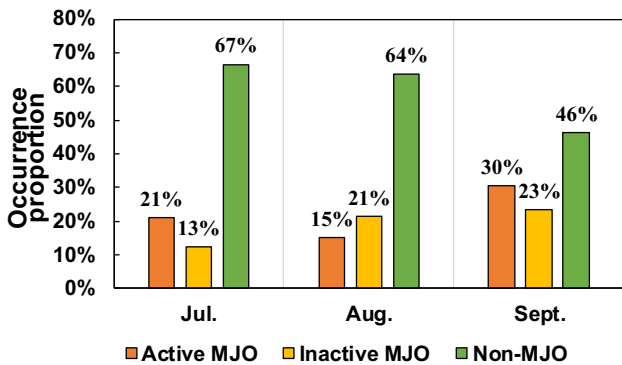


**Fig. 10** Occurrence proportion (%) of active MJO (orange bars), inactive MJO (yellow bars), and non-MJO (green bars) events for J–A–S during La Niña developing years

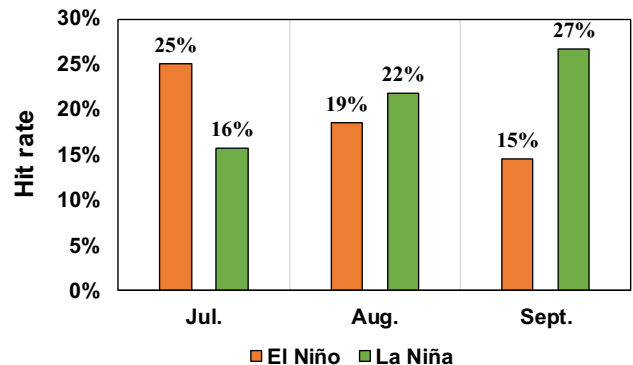
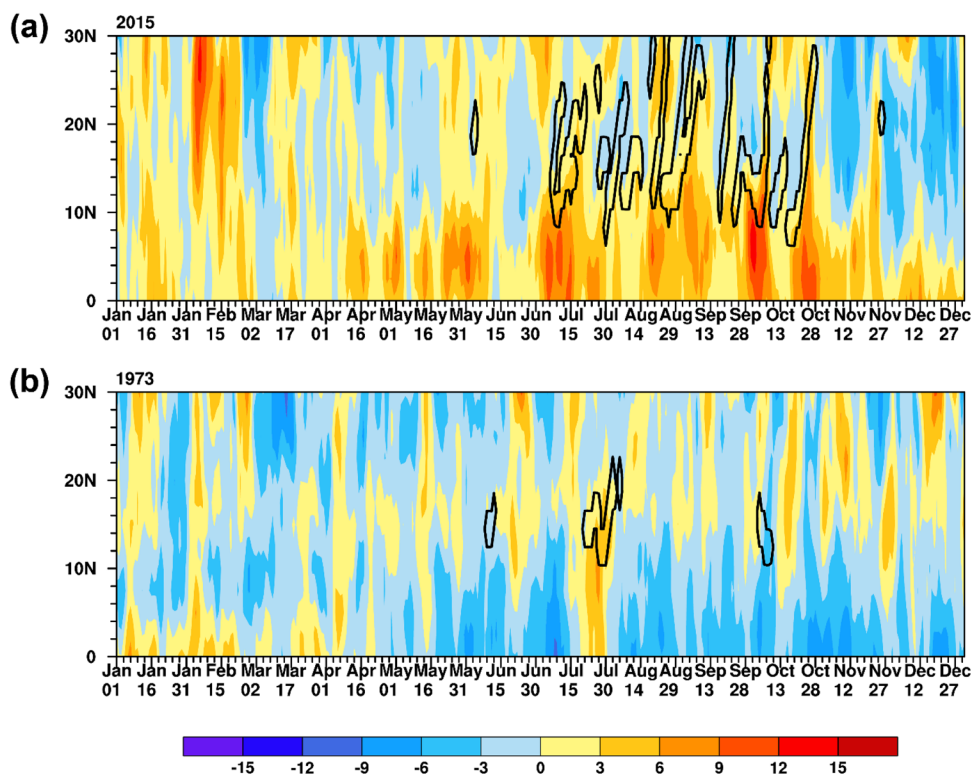


**Fig. 11** Hit rate (%) of MJO and ACE events for J–A–S during El Niño (orange bars) and La Niña (green bars) developing years

**Fig. 12** Latitude–time Hovmöller diagram (along 125°W–180°) of zonal wind anomalies (shading,  $m s^{-1}$ ) in the years of 2015 (El Niño year) and 1973 (La Niña year). Black contours indicate the 1 knot<sup>2</sup> isoline of the ENP ACE, representing the TC activities



and inactive MJO events during J–A–S are ~22% and ~19%, respectively. The non-MJO events occur most frequently (~59%). These results indicate that the feedback relationship between ENP TCs and ENSO intensity over interannual timescales might be independent of the MJO events. In addition, the hit rates between ENP ACE and MJO events (i.e., the ratio of days in which the ACE anomaly correctly matches the phase of the MJO event: positive ACE anomaly is for the active MJO event and negative ACE anomaly for the inactive MJO event) during J–A–S El Niño and La Niña events were explored further. As can be seen from Fig. 11,

for El Niño events, the hit rates for J–A–S are around 25%, 19%, and 15%, respectively. For La Niña events, the hit rates for J–A–S are around 16%, 22% and 27%, respectively. Overall, the hit rates remain low regardless of El Niño or La Niña events. All of this evidence supports the conclusion that the MJO might play a small role in the feedback relationship between ENP TCs and ENSO intensity over interannual timescales.

### 5 Possible mechanisms how ENP TCs affect ENSO intensity

Previous study (Wang et al. 2019b) showed that the possible pathways that TC over the western North Pacific modulates the ENSO are by changing the Walker circulation and the thermocline. Here, the possible mechanisms how ENP TCs affect ENSO intensity are further explored based on these two pathways.

Firstly, the characteristics of daily TCs are checked. The years of 2015 and 1973 are the typical El Niño and La Niña years, respectively. Here, taking the relationship between the daily zonal wind anomalies at the 850-hPa atmospheric level and TC activities during 2015 and 1973 as examples (Fig. 12), similar to the TCs over the western North Pacific (Wang et al. 2019b), there are obviously anomalous westerlies at the southern flank of TCs. Meanwhile, the centers of anomalous westerlies shift to north with the northward

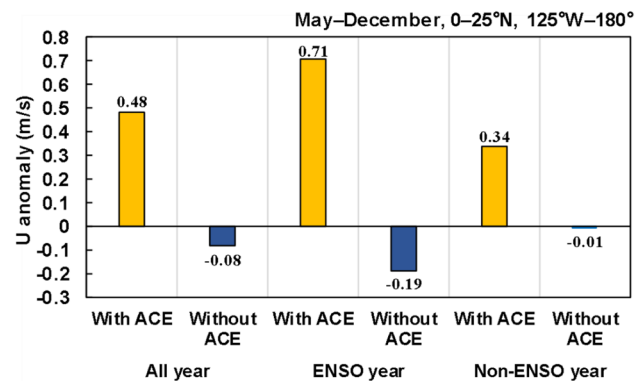


**Fig. 13** Average zonal wind anomalies with/without the ENP ACE in the region of 0°–25°N, 125°W–180° from May to December in the period of 1970–2020, and the corresponding ENSO and Non-ENSO years

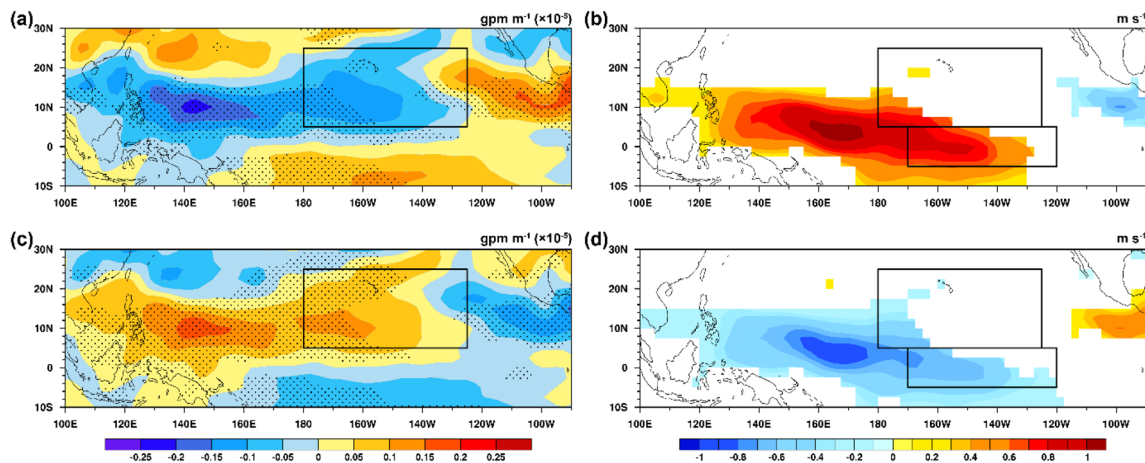


**Fig. 14** J–A–S geopotential height gradient ( $\text{gpm m}^{-1}$ , **a** and **c**) and zonal wind ( $\text{m s}^{-1}$ , **b** and **d**) anomalies at the 850-hPa level related to the J–A–S ACE during El Niño (**a** and **b**) and La Niña (**c** and **d**) events in the period 1970–2020. In **a** and **c**, the stippled regions denote the statistical significance of regression and composite analysis

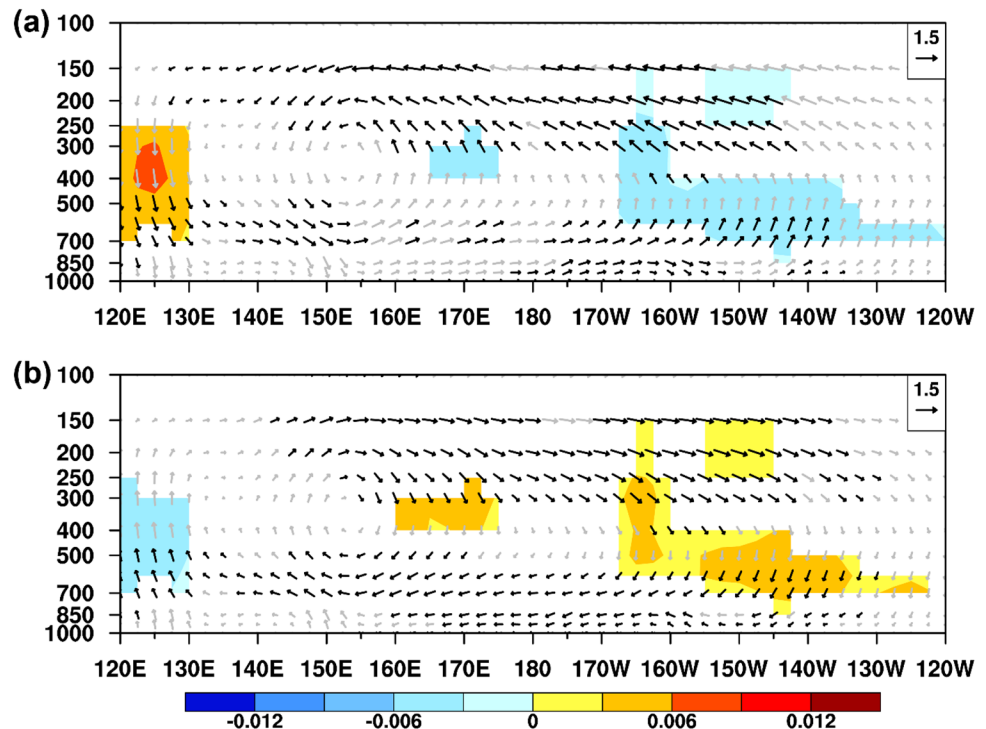
ses are both above the 95% confidence level. In **b** and **d**, shading indicates the statistical significance of regression and composite analyses are both above the 95% confidence level. The black rectangles denote the key domain of ACE ( $5^{\circ}$ – $25^{\circ}$ N,  $125^{\circ}$ W– $180^{\circ}$ ) and Niño 3.4 region ( $5^{\circ}$ S– $5^{\circ}$ N,  $120^{\circ}$ – $170^{\circ}$ W)

movements of TCs. What’s more important, during TC season (May – December), the intensification of the ENP TCs to the anomalous westerlies always exists whether the ENSO happens or not (Fig. 13), which means it is the inherent attribute of TCs over the ENP.

Previous studies (Keen 1982; Wang et al. 2019b) have proved that the influence of TCs on their surrounding environment could last for a while; And the accumulated effects of TCs on the wind fields works by the tropical

semi-geostrophic adjustment on the interannual timescale. During El Niño event, the mean ENP ACE anomaly in J–A–S is about  $237.06 \text{ knot}^2$ , which leads to the negative anomalies of the 850-hPa geopotential height gradient in J–A–S, especially the southern flank of the key domain of ACE (Fig. 14a). Thus, there are the evidently anomalous westerlies at 850-hPa in this region (Fig. 14b). And the area of the anomalous zonal wind is consistency with the composite result of daily TC activity in the Fig. 12. The

**Fig. 15** J–A–S wind (vectors) and the vertical  $p$ -velocity (shading,  $\text{Pa s}^{-1}$ ) anomalies in the vertical–zonal plane over  $5^{\circ}$ S– $5^{\circ}$ N related to the J–A–S ACE in the period 1970–2020 during El Niño (**a**) and La Niña (**b**) events. Vectors are obtained by the zonal wind anomalies and magnified vertical  $p$ -velocity ( $\times(-200)$ ). Shading and black vectors indicate the statistical significance of regression and composite analyses are both above the 95% confidence level



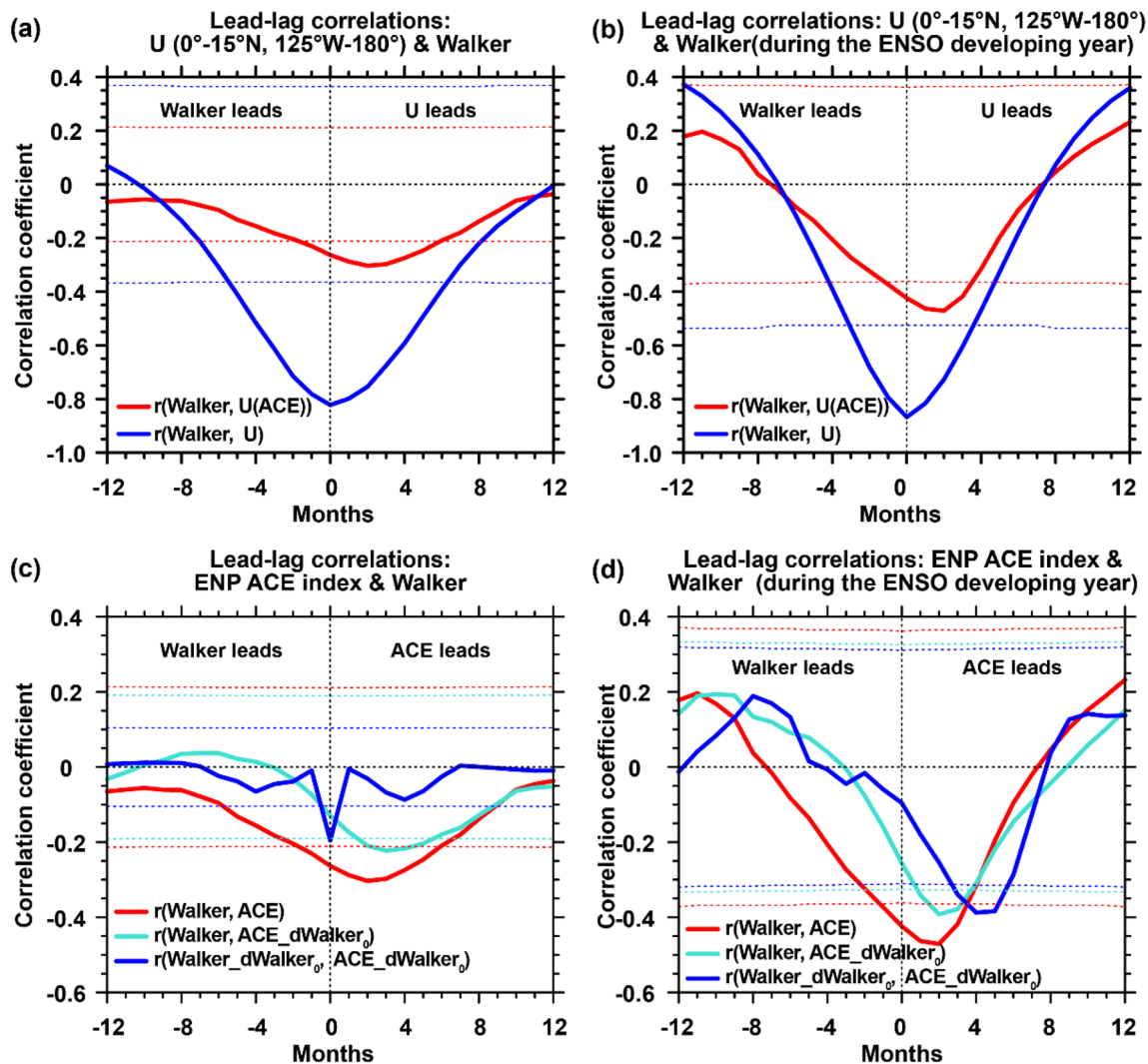


**Fig. 16** Lead-lag correlations between the Walker circulation index and regionally zonal wind anomalies ( $0^{\circ}$ – $15^{\circ}$ N,  $125^{\circ}$ W– $180^{\circ}$ , at the 850-hPa level), and the ENP ACE index ( $5^{\circ}$ – $25^{\circ}$ N,  $125^{\circ}$ W– $180^{\circ}$ ) and Walker circulation index in the period of 1970–2020. **a** Lead-lag correlations between the Walker circulation index and regionally zonal wind anomalies, Walker and  $U$  indicate the original series of the Walker circulation index and the regionally zonal wind anomalies, respectively; ACE indicate the original series of the ENP ACE index;  $U(\text{ACE})$  denote the regionally zonal wind anomalies related to the ENP ACE. Solid lines indicate the lead-lag correlation coefficients,

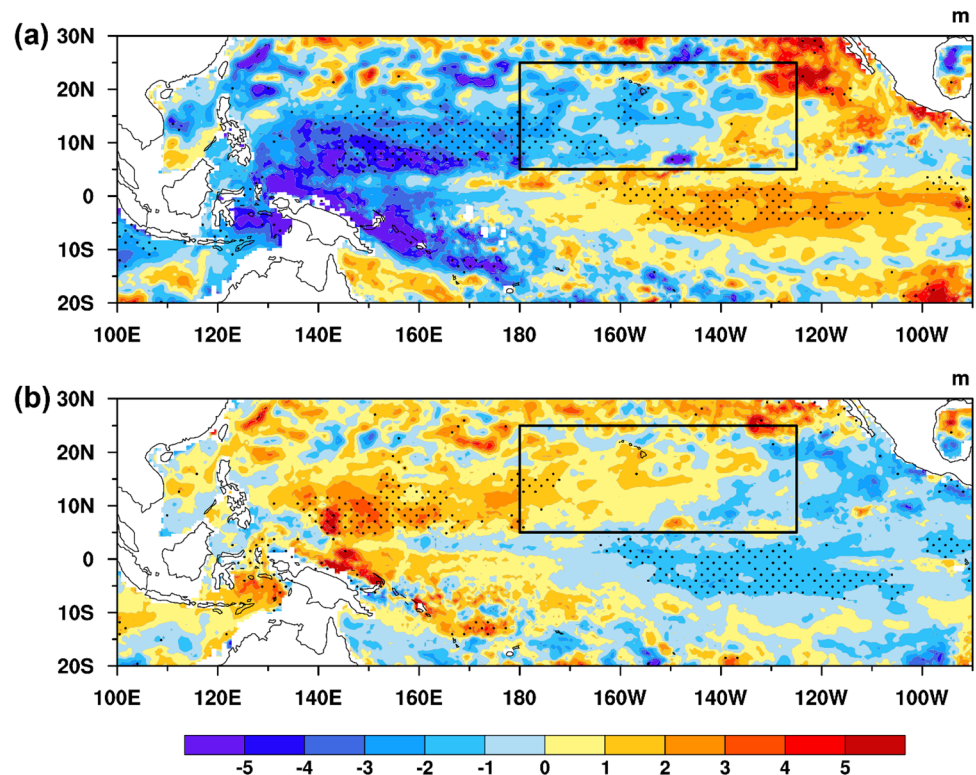
anomalous zonal winds near the equator would change the Walker circulation. Hence, there is a reversed Walker circulation anomaly under the action of these ENP ACE in J–A–S (Fig. 15a). This feature will enhance the eastward transport of warm sea water over the western Pacific Ocean, thus the intensity of El Niño event is strengthened. During La Niña events, the mean ENP ACE anomaly in J–A–S is about  $-199.16 \text{ knot}^2$ , on the condition of lack of TCs, there are the positive geopotential height gradient anomalies

and dashed lines indicate the corresponding significance at the 99% confidence level based on Student's  $t$  test using the effective number of degrees of freedom. **b** As in **a**, but for the timeseries during the ENSO developing years. **c** As in **a**, but for the ENP ACE index and the Walker circulation index.  $\text{ACE\_dWalker}_0$  and  $\text{Walker\_dWalker}_0$  denote the ENP ACE index and the Walker circulation index, respectively, which the preceding (3 months earlier) Walker circulation index is removed. **d** As in **c** but for the timeseries during the ENSO developing years

at the 850-hPa level (Fig. 14c), which further leading to the anomalous easterlies on the southern flank of the key domain of ACE (Fig. 14d). Thus, there is a Walker circulation anomaly (Fig. 15b), which supports westward transport of cold sea water over the eastern Pacific Ocean, further intensifying the development of the La Niña event. Otherwise, more evidences are provided in the time relationship among the anomalous zonal winds, Walker circulation and ACE indices: as shown in Figs. 16a–b, in general, there is a



**Fig. 17** As in Fig. 14, but for the depth of the 20 °C isotherm anomalies (shading, m) in the period 1970–2010. The stippled regions denote the statistical significance of regression and composite analyses are both above the 95% confidence level. The black rectangles denote the key ENP ACE regions (5°–25°N, 125°W–180°)



simultaneous change between the anomalous Walker circulation and the low-level zonal wind (0°–15°N, 125°W–180°, the key area which TCs affect anomalous zonal wind in the Fig. 14). However, the change of the low-level zonal wind anomaly related to the ENP ACE leads Walker circulation anomaly about 2 months. And the modulation of the ENP ACE on the anomalous Walker circulation reaches its peak after 2–3 months (Fig. 16c), and this lead relationship still exists after even removing the autocorrelation of the Walker circulation with its value 3 months earlier and the effects of the preceding Walker circulation on the ENP ACE. It needs to be noted that the simultaneous correlation between the Walker circulation after removing the preceding its own signal and the ACE index after removing the signal of the preceding Walker circulation is maximum, while the lead signal of ACE relative to Walker circulation is evident during the ENSO developing year (Fig. 16d). This might result from the ENP ACE in the non-ENSO year. In the non-ENSO year, there are small ENP ACE anomalies. Meanwhile, the atmospheric response is quick. Therefore, the cumulative effect of these ACE anomalies might be not enough to maintain the continuous change of the Walker circulation. Of course, this feature needs to be further study.

For thermocline, during El Niño event, there is a positive anomaly in the thermocline over the region south of key domain of ENP ACE under the action of ENP ACE in J-A-S,

which means the thermocline here is deepened (Fig. 17a); and the east–west thermocline gradient decreases. On the contrary, during La Niña, the lack of TCs leads that the thermocline over the region south of key domain of ENP ACE is shallowed in J–A–S, and the east–west thermocline gradient increases (Fig. 17b). Time relationship between the thermocline and thermocline gradient gives more evidence (Figs. 18a, b): the change of eastern thermocline leads the change of east–west thermocline gradient by ~ 1 month. And the change of eastern thermocline related to the ENP ACE brings this leading feature to ~ 3 months, which further verify the important role of ENP ACE in the change of thermocline. Furthermore, results indicate that the change of the east–west thermocline gradient related to the ENP ACE results essentially from the low-level zonal wind anomalies caused by the ENP TCs (Fig. 19). The modulation of the anomalously zonal wind at 850-hPa on the thermocline gradient further helps to the eastward (westward) transport of warm (cold) sea water during El Niño (La Niña) events. Overall, the oceanic response is slow relative to atmospheric response, the modulation of the ENP ACE on the anomalous east–west thermocline gradient reaches its peak after 3–4 months (Figs. 18c, d). And this lead relationship is independent with the autocorrelation of the east–west thermocline gradient with its value 3 months earlier and the effects of the preceding east–west thermocline gradient on the ENP ACE. Combined the lead times of ENP ACE to the anomalous Walker circulation (2–3 months), the ENP ACE leads

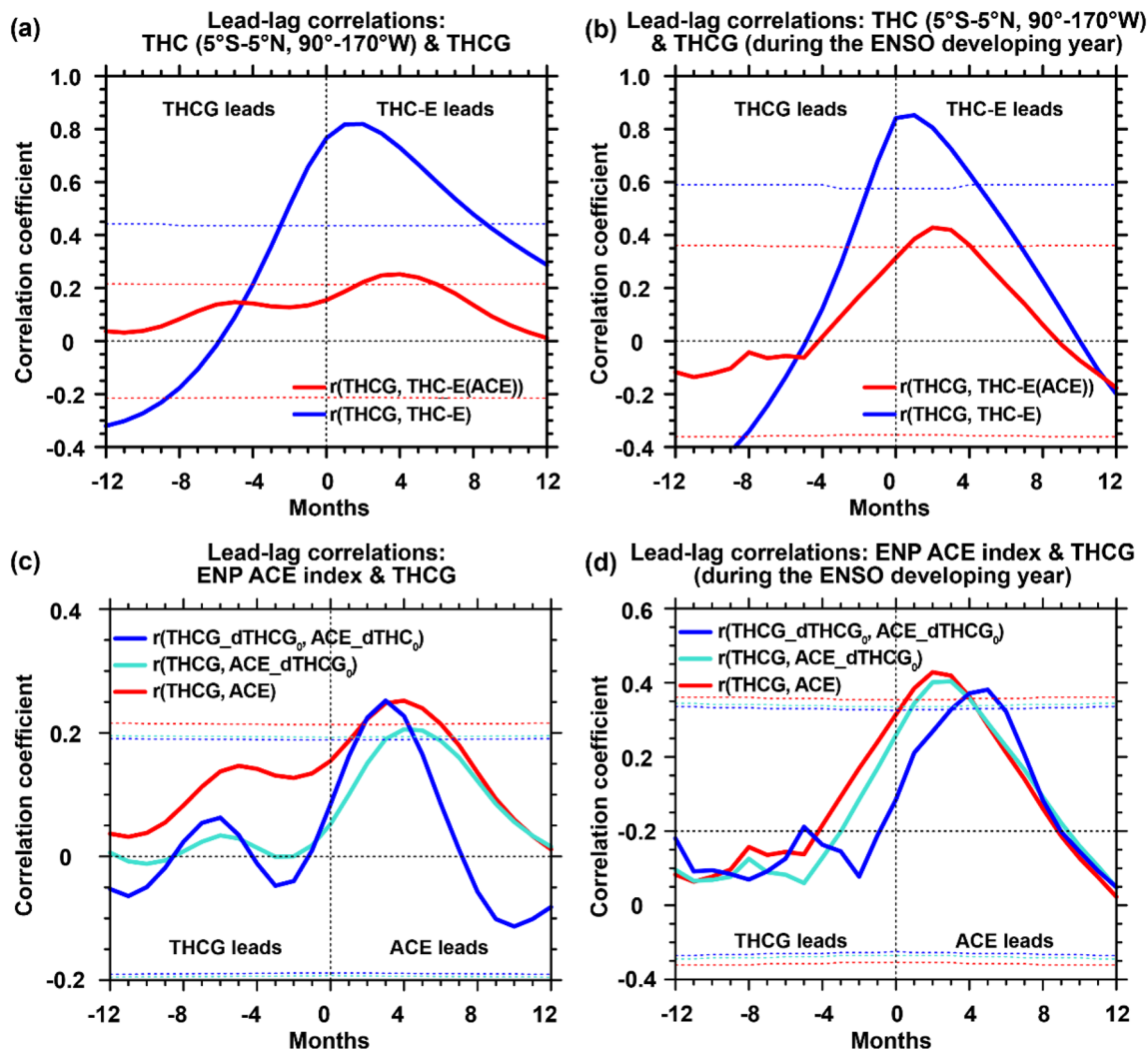


**Fig. 18** As in Fig. 16, but for the eastern thermocline (5°S–5°N, 90°–170°W) and the east–west thermocline gradient index (a and b), and ENP ACE index and the east–west thermocline gradient index (c and d) in the period of 1970–2010. THC-E, THCG and ACE indicate the original series of the eastern thermocline, the east–west thermocline

gradient and ENP ACE indices, respectively; THC-E(ACE) denotes the eastern thermocline related to the ENP ACE; ACE\_dTHCG<sub>0</sub> and THCG\_dTHCG<sub>0</sub> denote the ENP ACE and the east–west thermocline gradient indices, respectively, which the preceding (3 months earlier) east–west thermocline gradient index is removed

SST anomalies reaches its peak after 3 months during ENSO events, which is consistent with results shown in Fig. 2.

## 6 Summary and discussion

This study investigates the possible feedback of ENP TCs on the ENSO intensity. The observed and model results indicate that ENP TCs can significantly affect ENSO intensity 3 months later by way of ACE, and especially those TCs that develop during the J–A–S period. Generally, the greater the preceding ENP ACE, the stronger the El Niño; and the smaller the preceding ENP ACE, the stronger the La Niña. This feedback is independent from the persistence of the SST in the Niño 3.4 region and MJO. The impact of ENP TCs on El Niño

might be about equal to their impact on La Niña, but is smaller than the effect of SST persistence. MJO does little to change this impact. The modulated extent of the ENP TCs during J–A–S to Niño 3.4 index during O–N–D could reach ~7–22% during El Niño, and ~6–19% for La Niña. This feedback of ENP TCs on ENSO intensity is caused by the modulation of ENP TCs on the anomalous zonal wind at the low-level atmospheric layer, the joint impacts of the low-level zonal wind anomalies on the Walker circulation and the east–west thermocline gradient lead to the time characteristics that ENP TCs lead ENSO intensity by about 3 months.

Most ENP TCs do not make landfall; therefore, they have received less attention, particularly those TCs that develop away from the mainland. The results from this study remind us that these TCs are worthy of further study, and

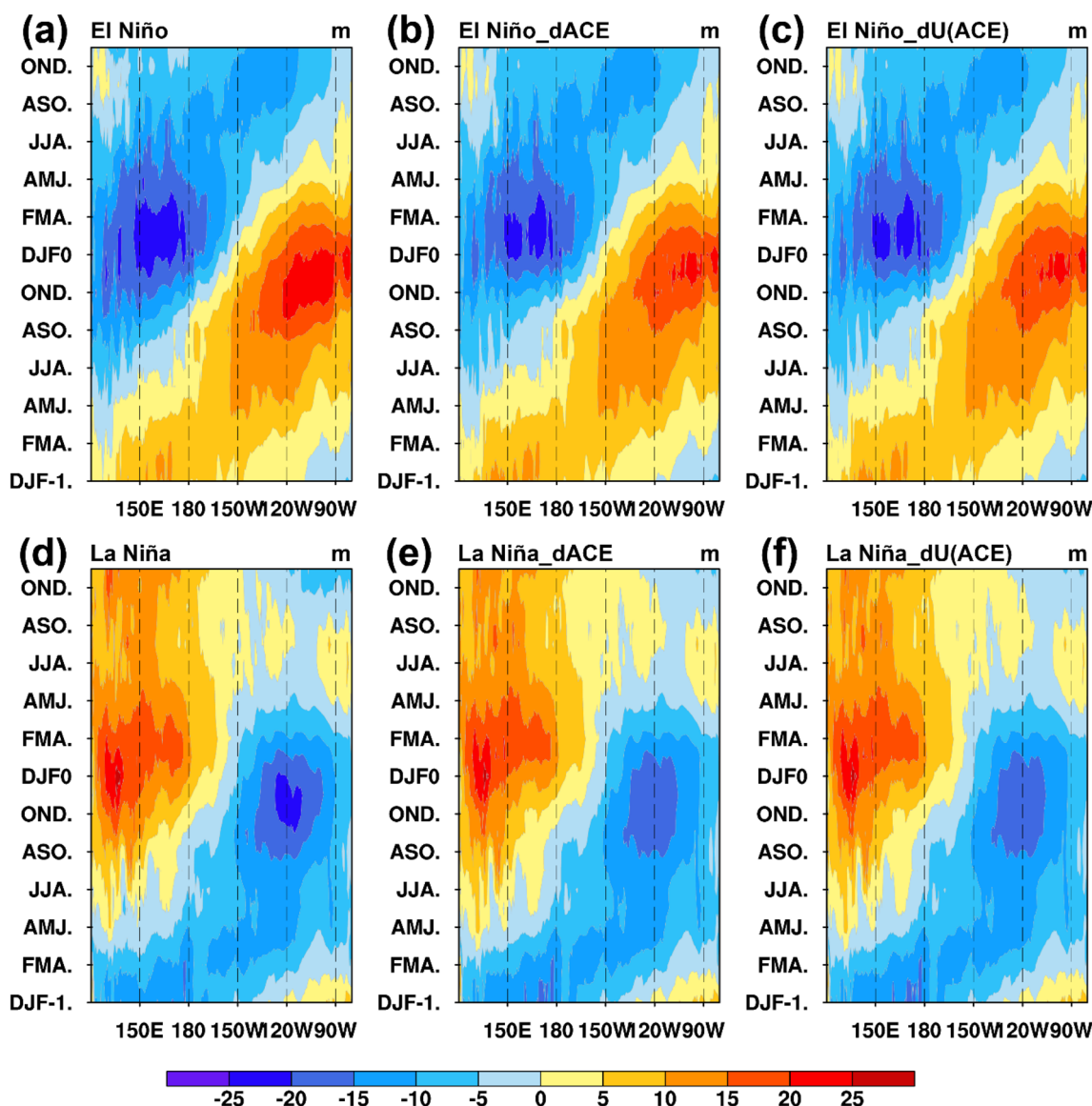


**Fig. 19** Spatial evolution of zonally (along 5°S–5°N) anomalous depth of the 20 °C isotherm (i.e., thermocline, shading, m) during ENSO events in the period 1970–2010. **a** Zonal thermocline depth anomalies during El Niño. DJF–1 and DJF0 represent the December–February of the previous year and the year when the peak of El Niño

occurs, respectively. **b** As in **a**, but for the zonal thermocline depth anomalies removing the effect of the preceding ENP ACE anomalies. **c**, As in **b** but for the zonal thermocline depth anomalies removing the effect of the preceding zonal wind anomalies related to the ENP ACE. **d–f**, As in **a–c**, but for La Niña events

the climatic effect caused by them should not be neglected. Sometimes, their climate effect might exceed their direct influence, although they do not make landfall. Here, it should be noted that this study just removes the linear influences of SST persistence and MJO on the feedback of ENP TCs on ENSO intensity. The influence of ENP ACE and other factors on ENSO intensity could not be separated completely because of the limitations of the current models (Hu et al. 2019; Wang et al. 2019b; Ren et al. 2020; Fang and Zheng 2021; Vidale et al. 2021). Much research is necessary. In addition, by considering the previous study of (Wang et al.

2019b), we can conclude that the impact of ENP TCs on ENSO is smaller than that of TCs over the western North Pacific, and the pathway that ENP TCs affect ENSO is simpler. This might be related to the differences in the magnitude of ACE between the two basins. Also, it is easy to see that there might be some similarities between TCs over the western and eastern North Pacific. For example, TCs in these two basins both lead the Niño 3.4 index by about 3 months. This implies that the TCs over the western North Pacific and ENP might jointly contribute to the intensity of ENSO events; however, of course, this requires further study.

## Appendix I : Abbreviations occurred in the text or figures

Abbreviations	Illustrations	Related figures
ENSO	El Niño–Southern Oscillation	–
SST	Sea surface temperature	
TC	Tropical cyclone	
ENP	Eastern North Pacific	
ACE	Accumulated cyclone energy	
MJO	Madden–Julian Oscillation	
J-A-S	July, August and September	
O-N-D	October, November and December	
N3.4	Niño 3.4 index	Figures 2, 3, 4, 5, 6
N3.4 <sub>0</sub>	Preceding (three months earlier) Niño 3.4 index	
N3.4_dN3.4 <sub>0</sub>	Niño 3.4 index after removing the preceding Niño 3.4 index	Figure 2
ACE_dN3.4 <sub>0</sub>	ENP ACE index after removing the preceding Niño 3.4 index	
N3.4(N3.4 <sub>0</sub> )	Niño 3.4 indices associated with N3.4 <sub>0</sub>	Figures 3, 4, 5, 6
N3.4 <sub>0</sub> <sup>*</sup>	Preceding Niño 3.4 index after removing the preceding ENP ACE, i.e., ACE-independent Niño 3.4 index	
N3.4(N3.4 <sub>0</sub> <sup>*</sup> )	Niño 3.4 indices associated with N3.4 <sub>0</sub> <sup>*</sup>	
ACE <sub>0</sub>	Preceding ENP ACE anomalies	
N3.4(ACE <sub>0</sub> )	Niño 3.4 indices associated with ACE <sub>0</sub>	
ACE <sub>0</sub> <sup>*</sup>	Preceding ENP ACE anomalies after removing the preceding Niño 3.4 index, i.e., Niño 3.4 index-independent ACE	
N3.4(ACE <sub>0</sub> <sup>*</sup> )	Niño 3.4 indices associated with ACE <sub>0</sub> <sup>*</sup>	
ACE <sub>0</sub> + N3.4 <sub>0</sub>	Factor consists of the preceding ENP ACE and Niño 3.4 index	Figures 4, 5, 6
N3.4(ACE <sub>0</sub> + N3.4 <sub>0</sub> )	Niño 3.4 index associated with ACE <sub>0</sub> + N3.4 <sub>0</sub> ,	
ACE <sub>0</sub> <sup>*</sup> + N3.4 <sub>0</sub>	Factor consists of the preceding ACE <sub>0</sub> <sup>*</sup> and Niño 3.4 index	
N3.4(ACE <sub>0</sub> <sup>*</sup> + N3.4 <sub>0</sub> )	Niño 3.4 index associated with ACE <sub>0</sub> <sup>*</sup> + N3.4 <sub>0</sub>	
U	Regionally zonal wind anomalies (0°–15°N, 125°W–180°)	Figure 16
Walker	Walker circulation index	
U(ACE)	Regionally zonal wind anomalies related to the ENP ACE	
ACE_dWalker <sub>0</sub>	ENP ACE index which the preceding Walker circulation index is removed	
Walker_dWalker <sub>0</sub>	Walker circulation index which the preceding Walker circulation index is removed	
THC-E	Eastern thermocline (5°S–5°N, 90°–170°W)	Figure 18
THC-E(ACE)	Eastern thermocline related to the ENP ACE	
THCG	East–west thermocline gradient index	
ACE_dTHCG <sub>0</sub>	ENP ACE which the preceding east–west thermocline gradient index is removed	
THCG_dTHCG <sub>0</sub>	East–west thermocline gradient which the preceding east–west thermocline gradient index is removed	

## Appendix II: Details of experimental set-up

Firstly, because of the limitations of the current models, it's still a great challenge to examine the effect of TC on ENSO directly using TC/ACE as the initial forcing (Hu et al. 2019; Wang et al. 2019b; Ren et al. 2020; Fang and Zheng 2021; Vidale et al. 2021). Secondly, previous studies (Wang et al. 2019b; Wang and Li 2022a, b, c) have

shown that TCs can affect ENSO by modulating wind field. Thirdly, LDEO<sub>5</sub> can simulate the response of SST to anomalous wind field, and forecast subsequent SST during ENSO events (Chen et al. 2004; Wang et al. 2019b; Gao et al. 2020). Hence, the experiments applied the surface horizontal wind anomalies related to the different impact factors (based on the simultaneous regression) as initial forcing.

Experiments	Details	Illustrations
Experiment I	Step 1, the surface horizontal wind anomalies related to Niño 3.4 index from 1970 to 2020, as an initial forcing, are added to simulate Niño 3.4 index;	
	Step 2, the discrepancy between the observed and simulated Niño 3.4 indices is corrected	Ensure a better simulation of LDEO <sub>5</sub> on Niño 3.4 index
	Step 3, the simulated Niño 3.4 index after correction are employed to predict Niño 3.4 index three months later in LDEO5	The role of SST-persistence in the SST three months later
	Step 4, Select the forecasting Niño 3.4 index during ENSO developing year	Obtain the Fig. 5a, g
Experiment II	Step 1, the surface horizontal wind anomalies related to Niño 3.4 index after removing the signal of simultaneous ENP ACE (i.e. ACE-independent Niño 3.4 index) from 1970 to 2020, as an initial forcing, are added to simulate Niño 3.4 index;	
	Step 2, the discrepancy between the observed and simulated Niño 3.4 indices is corrected using the correction coefficient obtained by the experiment I	Same correction coefficient as Experiment I can ensure obtained the relative contribution of SST persistence and SST persistence after removing the influence of ENP ACE
	Step 3, the simulated Niño 3.4 index after correction are employed to predict Niño 3.4 index three months later in LDEO5	
	Step 4, Select the forecasting Niño 3.4 index during ENSO developing year	Obtain the Fig. 5b, h
Experiment III	Step 1, the surface horizontal wind anomalies related to the ENP ACE from 1970 to 2020, as an initial forcing, are added to simulate Niño 3.4 index;	
	Step 2, the discrepancy between the observed and simulated Niño 3.4 indices is corrected using the correction coefficient obtained by the experiment I	Same correction coefficient as Experiment I can ensure obtained the relative contribution of ACE and the aforementioned factors
	Step 3, the simulated Niño 3.4 index after correction are employed to predict Niño 3.4 index three months later in LDEO5	
	Step 4, Select the forecasting Niño 3.4 index during ENSO developing year	Obtain the Fig. 5c, i

Experiments	Details	Illustrations
Experiment IV	<p>Step 1, the surface horizontal wind anomalies related to the ENP ACE after removing the signal of simultaneous Niño 3.4 index (Niño 3.4 index-independent ACE) from 1970 to 2020, as an initial forcing, are added to simulate Niño 3.4 index;</p> <p>Step 2, the discrepancy between the observed and simulated Niño 3.4 indices is corrected using the correction coefficient obtained by the experiment I</p> <p>Step 3, the simulated Niño 3.4 index after correction are employed to predict Niño 3.4 index three months later in LDEO5</p> <p>Step 4, Select the forecasting Niño 3.4 index during ENSO developing year</p>	<p>Same correction coefficient as Experiment I can ensure obtained the relative contribution of ACE after removing the signal of simultaneous Niño 3.4 SST and the aforementioned factors</p> <p>Obtain the Fig. 5d, j</p>
Experiment V	<p>Step 1, the surface horizontal wind anomalies related to the Niño 3.4 index and ENP ACE from 1970 to 2020, as an initial forcing, are added to simulate Niño 3.4 index;</p> <p>Step 2, the discrepancy between the observed and simulated Niño 3.4 indices is corrected using the correction coefficient obtained by the experiment I</p> <p>Step 3, the simulated Niño 3.4 index after correction are employed to predict Niño 3.4 index three months later in LDEO5</p> <p>Step 4, Select the forecasting Niño 3.4 index during ENSO developing year</p>	<p>Same correction coefficient as Experiment I can ensure obtained the relative contribution of joint factor (Niño 3.4 index and ENP ACE) and the aforementioned factors</p> <p>Obtain the Fig. 5e, k</p>
Experiment VI	<p>Step 1, the surface horizontal wind anomalies related to ACE-independent Niño 3.4 index and ENP ACE from 1970 to 2020, as an initial forcing, are added to simulate Niño 3.4 index;</p> <p>Step 2, the discrepancy between the observed and simulated Niño 3.4 indices is corrected using the correction coefficient obtained by the experiment I</p> <p>Step 3, the simulated Niño 3.4 index after correction are employed to predict Niño 3.4 index three months later in LDEO5</p> <p>Step 4, Select the forecasting Niño 3.4 index during ENSO developing year</p>	<p>Same correction coefficient as Experiment I can ensure obtained the relative contribution of joint factor (ACE-independent Niño 3.4 index and ENP ACE) and the aforementioned factors</p> <p>Obtain the Fig. 5f, l</p>
Experiments VII and VIII are similar to VI, but for the joint factors consist of ACE and Niño 3.4 index-independent ACE, and ACE-independent Niño 3.4 index and Niño 3.4 index-independent ACE, respectively		

**Acknowledgements** This work is jointly supported by the National Natural Science Foundation of China (42192555, 42105014), the China Postdoctoral Science Foundation (2021T140302, 2021M701652) and the Fundamental Research Funds for the Central Universities (201962009).

**Author contributions** Z-MT and QYW designed the study and contributed to the data analysis, interpretation, and writing of the paper.

**Funding** This work is jointly supported by the National Key R&D Program of China under Grants 2017YFC1501601, the National Natural Science Foundation of China (61827901, 42105014), the China

Postdoctoral Science Foundation (2021T140302, 2021M701652) and the Fundamental Research Funds for the Central Universities (201962009).

**Data availability** TCs dataset is available online at <https://www.ncdc.noaa.gov/ibtracs/>. The daily SST data is available online at <https://cds.climate.copernicus.eu/cdsapp#!/home>. The daily OLR data is available online at [https://psl.noaa.gov/data/gridded/data.interp\\_OLR.html](https://psl.noaa.gov/data/gridded/data.interp_OLR.html). The monthly wind dataset is available online at <https://psl.noaa.gov/data/gridded/data.ncep.reanalysis.pressure.html>. The monthly SST data is available online at <https://www.esrl.noaa.gov/psd/data/gridded/data.noaa.ersst.v5.html>. Ocean variables are available online at <http://apdrc.soest.hawaii.edu/las/v6/dataset?catitem=4867>.

**Code availability** Computer code used for the analysis was written in NCL, all types of figures that occur in this study can be found in NCL application examples (available online at <https://www.ncl.ucar.edu/Applications/>). More specific codes in this study are available to readers upon request.

#### Declaration

**Conflicts of interest** The authors declare no competing interests.

## References

- Alexander MA, Blade I, Newman M, Lanzante JR, Lau NC, Scott JD (2002) The atmospheric bridge: the influence of ENSO teleconnections on air-sea interaction over the global oceans. *J Clim* 15:2205–2231
- Balaguru K, Patricola CM, Hagos SM, Leung LR, Dong L (2020) Enhanced predictability of eastern north pacific tropical cyclone activity using the ENSO longitude index. *Geophys Res Lett* 47:e2020GL088849
- Bell GD, Halpert MS, Schnell RC, Higgins RW, Lawrimore J, Kousky VE, Tinker R, Thiaw W, Chelliah M, Artusa A (2000) Climate assessment for 1999. *B Am Meteorol Soc* 81:S1–S50
- Boucharel J, Jin F-F, England MH, Dewitte B, Lin II, Huang HC, Balmaseda MA (2016) Influence of oceanic intraseasonal Kelvin waves on eastern Pacific hurricane activity. *J Climate* 29:7941–7955
- Camargo SJ, Sobel AH (2005) Western North Pacific tropical cyclone intensity and ENSO. *J Clim* 18:2996–3006
- Camargo SJ, Robertson AW, Barnston AG, Ghil M (2008) Clustering of eastern North Pacific tropical cyclone tracks: ENSO and MJO effects. *Geochem Geophys Geosyst* 9:Q06V05
- Carton JA, Giese BS (2008) A reanalysis of ocean climate using simple ocean data assimilation (SODA). *Mon Weather Rev* 136:2999–3017
- Chand SS, Tory KJ, McBride JL, Wheeler MC, Dare RA, Walsh KJE (2013) The different impact of positive-neutral and negative-neutral ENSO regimes on Australian tropical cyclones. *J Clim* 26:8008–8016
- Chen D, Cane CM, Zebiak SE, Canizares R, Kaplan A (2000) Bias correction of an ocean-atmosphere coupled model. *Geophys Res Lett* 27:2585–2588
- Chen D, Cane MA, Kaplan A, Zebiak SE, Huang DJ (2004) Predictability of El Niño over the past 148 years. *Nature* 428:733–736
- Chu PS (2004) ENSO and tropical cyclone activity. Hurricanes and typhoons: past, present, and future. (ed). New York, Columbia University Press, pp 297–332
- Chu PS, Wang JX (1997) Tropical cyclone occurrences in the vicinity of Hawaii: are the differences between El Niño and non-El Niño years significant? *J Clim* 10:2683–2689
- Fang XH, Zheng F (2021) Effect of the air-sea coupled system change on the ENSO evolution from boreal spring. *Clim Dyn* 57:109–120
- Fedorov AV, Brierley CM, Emanuel K (2010) Tropical cyclones and permanent El Niño in the early Pliocene epoch. *Nature* 463:1066–U84
- Feng J, Li JP (2011) Influence of El Niño Modoki on spring rainfall over south China. *J Geophys Res-Atmos* 116:D13102
- Gao YQ, Liu T, Song XS, Shen ZQ, Tang YM, Chen DK (2020) An extension of LDEO5 model for ENSO ensemble predictions. *Clim Dynam* 55:2979–2991
- Gill AE (1980) Some simple solutions for heat-induced tropical circulation. *Q J Roy Meteor Soc* 106:447–462
- Guo YP, Tan Z-M (2018) Westward migration of tropical cyclone rapid-intensification over the Northwestern Pacific during short duration El Niño. *Nat Commun* 9:1507
- Gutzler DS, Wood KM, Ritchie EA, Douglas AV, Lewis MD (2013) Interannual variability of tropical cyclone activity along the Pacific coast of North America. *Atmosfera* 26:149–162
- Hu ZZ, Kumar A, Zhu JS, Peng PT, Huang BH (2019) On the challenge for ENSO cycle prediction: an example from NCEP climate forecast system, version 2. *J Clim* 32:183–194
- Huang BY, Thorne PW, Banzon VF, Boyer T, Chepurin G, Lawrimore JH, Menne MJ, Smith TM, Vose RS, Zhang HM (2017) Extended reconstructed sea surface temperature, version 5 (ERSSTv5): upgrades, validations, and intercomparisons. *J Clim* 30:8179–8205
- Irwin RP, Davis RE (1999) The relationship between the Southern Oscillation Index and tropical cyclone tracks in the eastern North Pacific. *Geophys Res Lett* 26:2251–2254
- Jiang XA, Zhao M, Waliser DE (2012) Modulation of tropical cyclones over the eastern Pacific by the intraseasonal variability simulated in an AGCM. *J Clim* 25:6524–6538
- Jien JY, Gough WA, Butler K (2015) The influence of El Niño–Southern Oscillation on tropical cyclone activity in the eastern North Pacific basin. *J Clim* 28:2459–2474
- Jin F-F, Boucharel J, Lin II (2014) Eastern Pacific tropical cyclones intensified by El Niño delivery of subsurface ocean heat. *Nature* 516:82–U178
- Kalnay E, Kanamitsu M, Kistler R, Collins W, Deaven D, Gandin L, Iredell M, Saha S, White G, Woollen J, Zhu Y, Chelliah M, Ebisuzaki W, Higgins W, Janowiak J, Mo KC, Ropelewski C, Wang J, Leetmaa A, Reynolds R, Jenne R, Joseph D (1996) The NCEP/NCAR 40-year reanalysis project. *B Am Meteorol Soc* 77:437–471
- Keen RA (1982) The role of cross-equatorial tropical cyclone pairs in the Southern Oscillation. *Mon Weather Rev* 110:1405–1416
- Kim HK, Seo KH, Yeh SW, Kang NY, Moon BK (2020) Asymmetric impact of Central Pacific ENSO on the reduction of tropical cyclone genesis frequency over the western North Pacific since the late 1990s. *Clim Dyn* 54:661–673
- Kug JS, Jin F-F, An SI (2009) Two types of El Niño events: cold tongue El Niño and warm pool El Niño. *J Clim* 22:1499–1515
- Li JP, Wang QY, Li YJ, Zhang JW (2016) Review and perspective on the climatological research of tropical cyclones in terms of energetics. *J Beijing Normal Univ (Nat Sci)* 52:705–713
- Lian T, Chen D, Tang Y, Liu X, Feng J, Zhou L (2018) Linkage between westerly wind bursts and tropical cyclones. *Geophys Res Lett* 45:11431–11438
- Lian T, Ying J, Ren HL (2019) Effects of tropical cyclones on ENSO. *J Clim* 32:6423–6443
- Liebmann B, Smith CA (1996) Description of a complete (interpolated) outgoing longwave radiation dataset. *B Am Meteorol Soc* 77:1275–1277
- Madden RA (1986) Seasonal variations of the 40–50 day oscillation in the tropics. *J Atmos Sci* 43:3138–3158
- Madden RA, Julian PR (1972) Description of global-scale circulation cells in the tropics with a 40–50 day period. *J Atmos Sci* 29:1109–1123
- Madden RA, Julian PR (1994) Observations of the 40–50-day tropical oscillation—a review. *Mon Weather Rev* 122:814–837
- Maloney ED, Hartmann DL (2000) Modulation of eastern North Pacific hurricanes by the Madden–Julian oscillation. *J Clim* 13:1451–1460
- Puy M, Vialard J, Lengaigne M, Guilyardi E (2016) Modulation of equatorial Pacific westerly/easterly wind events by the Madden–Julian oscillation and convectively-coupled Rossby waves. *Clim Dyn* 46:2155–2178

- Pyper BJ, Peterman RM (1998) Comparison of methods to account for autocorrelation in correlation analyses of fish data (vol 55, pg 2127, 1998). *Can J Fish Aquat Sci* 55:2710–2710
- Ren HL, Zheng F, Luo JJ, Wang R, Liu MH, Zhang WJ, Zhou TJ, Zhou GQ (2020) A review of research on tropical air-sea interaction, ENSO dynamics, and ENSO prediction in China. *J Meteorol Res Prc* 34:43–62
- Striver RL, Huber M, Chafik L (2013) Excitation of equatorial Kelvin and Yanai waves by tropical cyclones in an ocean general circulation model. *Earth Syst Dyn* 4:1–10
- Sun C, Li JP, Feng J, Xie F (2015) A decadal-scale teleconnection between the North Atlantic Oscillation and subtropical eastern Australian rainfall. *J Clim* 28:1074–1092
- Vidale PL, Hodges K, Vanniere B, Davini P, Roberts MJ, Strommen K, Weisheimer A, Plesca E, Corti S (2021) Impact of stochastic physics and model resolution on the simulation of tropical cyclones in climate GCMs. *J Clim* 34:4315–4341
- Wang QY, Li JP (2022a) Feedback of tropical cyclones on El Niño diversity. Part I: phenomenon. *Clim Dyn* 59:169–184
- Wang QY, Li JP (2022b) Feedback of tropical cyclones on El Niño diversity. Part II: possible mechanism and prediction. *Clim Dyn* 59:715–735
- Wang QY, Li JP (2022c) Feedback of tropical cyclones over the western North Pacific on La Niña Flavor. *Geophys Res Lett* 49:e2021GL097210
- Wang CZ, Li CX, Mu M, Duan WS (2013) Seasonal modulations of different impacts of two types of ENSO events on tropical cyclone activity in the western North Pacific. *Clim Dyn* 40:2887–2902
- Wang CZ, Deser C, Yu J-Y, Di Nezio P, Clement A (2016) El Niño-Southern Oscillation (ENSO): a review. coral reefs of the eastern Pacific. In: Glynn PW, Manzello DP, Enochs IC (ed) Springer Science Publisher, pp 85–106
- Wang QY, Li JP, Li JY, Xue JQ, Zhao S, Xu YD, Wang YH, Zhang YZ, Dong D, Zhang JW (2019a) Modulation of tropical cyclone tracks over the western North Pacific by intra-seasonal Indo-western Pacific convection oscillation during the boreal extended summer. *Clim Dyn* 52:913–927
- Wang QY, Li JP, Jin F-F, Chan JCL, Wang CZ, Ding RQ, Sun C, Zheng F, Feng J, Xie F, Li YJ, Li F, Xu YD (2019b) Tropical cyclones act to intensify El Niño. *Nat Commun* 10:3793
- Wheeler MC, Hendon HH (2004) An all-season real-time multivariate MJO index: development of an index for monitoring and prediction. *Mon Weather Rev* 132:1917–1932
- Xie F, Li JP, Tian WS, Zhang JK, Sun C (2014) The relative impacts of El Niño Modoki, canonical El Niño, and QBO on tropical ozone changes since the 1980s. *Environ Res Lett* 9:064020
- Xie F, Zhang JK, Li XT, Li J, Wang T, Xu M (2020) Independent and joint influences of eastern Pacific El Niño-southern oscillation and quasi-biennial oscillation on Northern Hemispheric stratospheric ozone. *Int J Climatol* 40:5289–5307
- Yang S, Oh J (2018) Long-term changes in the extreme significant wave heights on the western North Pacific: Impacts of tropical cyclone activity and ENSO. *Asia-Pac J Atmos Sci* 54:103–109
- Zebiak SE, Cane MA (1987) A model El-Niño Southern Oscillation. *Mon Weather Rev* 115:2262–2278
- Zhan RF, Wang YQ, Zhao JW (2017) Intensified Mega-ENSO has increased the proportion of intense tropical cyclones over the western Northwest Pacific since the late 1970s. *Geophys Res Lett* 44:11959–11966

**Publisher's Note** Springer Nature remains neutral with regard to jurisdictional claims in published maps and institutional affiliations.

Springer Nature or its licensor (e.g. a society or other partner) holds exclusive rights to this article under a publishing agreement with the author(s) or other rightsholder(s); author self-archiving of the accepted manuscript version of this article is solely governed by the terms of such publishing agreement and applicable law.